JVST A
Journal of Vacuum Science & Technology A

ARTICLE

avs.scitation.org/journal/jva

Vapor-phase grafting of functional silanes on atomic layer deposited Al_2O_3

Cite as: J. Vac. Sci. Technol. A **41**, 032408 (2023); doi: 10.1116/6.0002364
Submitted: 15 November 2022 · Accepted: 27 March 2023 ·
Published Online: 24 April 2023

Vepa Rozyyev,[1,2,3] Rahul Shevate,[2] Rajesh Pathak,[2] Julia G. Murphy,[3,4] Anil U. Mane,[2,3] S. J. Sibener,[3,4] and Jeffrey W. Elam[2,3,a)]

AFFILIATIONS

[1]Pritzker School of Molecular Engineering, The University of Chicago, 5640 S. Ellis Ave Chicago, Illinois 60637
[2]Applied Materials Division, Argonne National Laboratory, Lemont, Illinois 60439
[3]Advanced Materials for Energy-Water Systems (AMEWS) Energy Frontier Research Center (EFRC), Lemont, Illinois 60439
[4]The James Franck Institute and Department of Chemistry, The University of Chicago, 929 E. 57th Street, Chicago, Illinois 60637

[a)]**Electronic mail:** jelam@anl.gov

ABSTRACT

Fundamental studies are needed to advance our understanding of selective adsorption in aqueous environments and develop more effective sorbents and filters for water treatment. Vapor-phase grafting of functional silanes is an effective method to prepare well-defined surfaces to study selective adsorption. In this investigation, we perform vapor phase grafting of five different silane compounds on aluminum oxide (Al_2O_3) surfaces prepared by atomic layer deposition. These silane compounds have the general formula $L_3Si–C_3H_6–X$ where the ligand, L, controls the reactivity with the hydroxylated Al_2O_3 surface and the functional moiety, X, dictates the surface properties of the grafted layer. We study the grafting process using *in situ* Fourier transform infrared spectroscopy and *ex situ* x-ray photoelectron spectroscopy measurements, and we characterize the surfaces using scanning electron microscopy, atomic force microscopy, and water contact angle measurements. We found that the structure and density of grafted aminosilanes are influenced by their chemical reactivity and steric constraints around the silicon atom as well as by the nature of the anchoring functional groups. Methyl substituted aminosilanes yielded more hydrophobic surfaces with a higher surface density at higher grafting temperatures. Thiol and nitrile terminated silanes were also studied and compared to the aminosilane terminated surfaces. Uniform monolayer coatings were observed for ethoxy-based silanes, but chlorosilanes exhibited nonuniform coatings as verified by atomic force microscopy measurements.

I. INTRODUCTION

The contamination of freshwater resources from existing and emerging water-based pollutants including pharmaceuticals, pesticides, and industrial waste is an urgent and global concern.[1,2] Among various remediation strategies, adsorptive removal is a simple and effective means to remove pollutants from water with high efficiency.[3] Fundamental research is needed to develop improved sorbents for water treatment that exhibit higher selectivity, improved reusability, and greater fouling resistance. To establish structure-function-property relationships in selective absorbing materials, it is crucial to synthesize materials with well-defined morphology and surface chemistry.[4] Covalent surface modification with alkyl silanes is one of the most commonly used methods to prepare well-defined functional surfaces.[5,6] Alkyl silanes have one or more ligands, L (e.g., L = —OCH_2CH_3, —OCH_3, or —Cl) attached to a central silicon atom that can react to anchor the molecule to a surface, and an alkyl group terminated with a functional moiety, X (e.g., X = —CN, —NH_2, —SH, or —C(=O)OR) selected to tune the chemistry of the functionalized surface [Fig. 1(a)]. The main advantage of silane functionalization is the rapid formation of stable siloxy bonds with surface hydroxyl groups on metal oxide substrates.[7] Alkyl silanes can be synthesized with a broad array of functional groups on the alkyl chain to create a variety of functional surfaces for applications including water treatment,[8,9] biosensing,[10] and antifouling materials.[11] Due to their simplicity, solution-phase silane reactions have been widely studied and extensively utilized in various applications.[12–14] For instance, Kujawski *et al.* reported on the solution-phase silanization of ceramic powders and membranes with hydrophobic alkyl silanes and

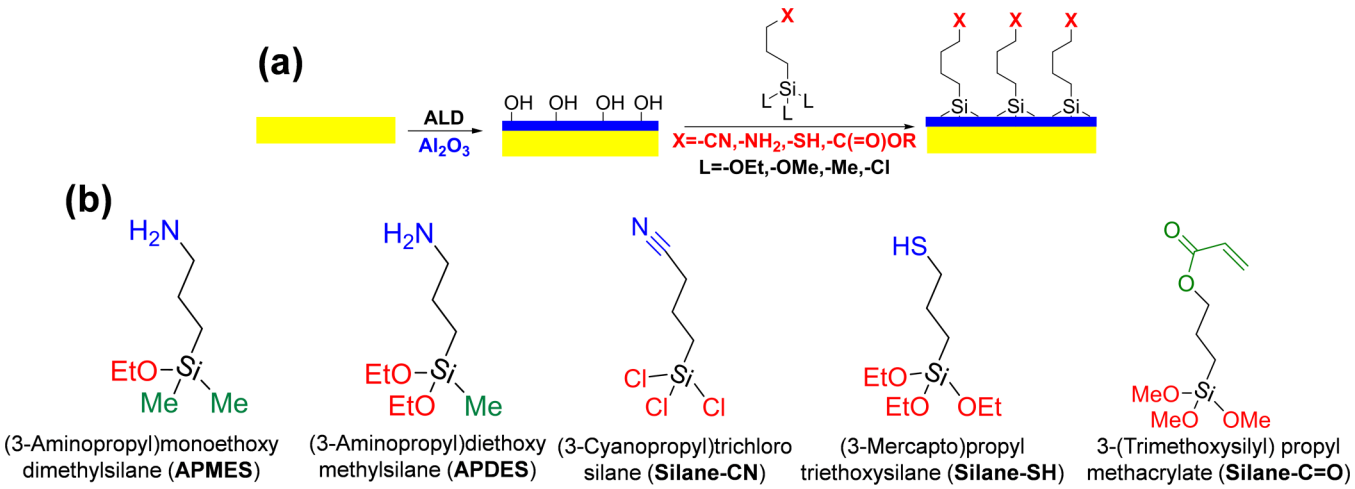

FIG. 1. (a) Reaction scheme for Al_2O_3 ALD and subsequent silanization. (b) Chemical structures of silane compounds studied in this work.

fluoroalkyl silanes.[15–18] These previous studies used longer chain fluorinated and nonfluorinated octyl silanes to functionalize metal oxide surfaces. However, to create uniform self-assembled monolayer films, vapor-phase reactions offer many advantages compared to solution-phase reaction methods.[19–21]

In addition to the surface chemistry of the grafted alkyl silane, the mesostructure of the underlying substrate also plays a significant role in establishing the properties of adsorbent materials such as pore size distribution, surface area, and permeance.[22–24] Atomic layer deposition (ALD) is a vapor-phase surface coating technique that is widely used to deposit thin films on substrates with complex geometries including nanoporous and high surface area powders and membranes.[25] ALD provides atomic scale control over thickness and composition and hence can be used to tune the pore size and surface chemistry of porous substrates.[26,27] ALD is an ideal method to prepare surfaces for silane modification, because metal oxides prepared by ALD typically have a high density of surface hydroxyls that react with the silane ligands and provide precise control over surface morphology.[28,29] The siloxy end of functional silanes will react with the surface hydroxyls of the ALD metal oxide such as Al_2O_3, while the functional moiety serves as an adsorption site for the removal of contaminants from water [Fig. 1(a)]. Vapor-phase silane modification can be carried out in the same reactor immediately following the ALD to avoid contamination of the freshly prepared surface upon air exposure. We have previously reported the monolayer functionalization of ALD Al_2O_3, ZnO, and TiO_2 surfaces with (3-aminopropyl)triethoxysilane (APTES).[30] In this study, the vapor-phase reactions were conducted under inert gas flow conditions that allowed us to study the mechanism of monolayer silane formation on the oxide surfaces using *in situ* measurements. We found that APTES reacts through different bonding configurations depending on the reaction temperature and the choice of ALD metal oxide. For instance, on TiO_2 APTES reacts through both the silyl group and the terminal amine group, but on Al_2O_3 and ZnO APTES reacts only through the silyl group. Following APTES adsorption at 100 °C on Al_2O_3, a higher surface coverage of one- and two-anchored aminosilanes was observed as compared to APTES adsorption at 200 °C where two- and three-anchored attachment was seen.

Here, we explore and compare the reactivity of different functional silanes under vapor-phase reaction conditions on ALD aluminum oxide (Al_2O_3). *In situ* Fourier-transform infrared (FTIR) spectroscopy and *ex situ* x-ray photoelectron spectroscopy (XPS), scanning electron microscopy (SEM), atomic force microscopy (AFM), and water contact angle (WCA) measurements were used to elucidate the chemical structure and surface properties of the modified surfaces. The silanes examined in this study are presented in Fig. 1(b) and include (3-aminopropyl)methyldiethoxysilane (APDES), (3-aminopropyl)monoethoxydimethylsilane (APMES), (3-mercaptopropyl)triethoxysilane (silane-SH), 3-(trimethoxysilyl) propylmethacrylate (Silane-C═O), and 3-cyanopropyltrichlorosilane (silane-CN). To investigate the effect of the number of ligands on the silane binding chemistry, we included APMES (1 ethoxy group) and APDES (two ethyoxy groups) which have a similar structure and functionality to APTES (3 ethoxy groups) from our previous work. The silane-CN and silane-C═O compounds were included to study the influence of ligand chemistry on the siloxane bond formation, and in combination with the silane-SH and amine-terminated compounds, provide a range of surface terminations. Finally, we have included compounds having ethoxy, methoxy, methyl, and chloride ligands to examine the effect of the ligand on the binding chemistry.

II. EXPERIMENT

A. Materials

The silane reagents used in this study were: (3-aminopropyl) dimethylmonoethoxysilane (APMES, 97%, Gelest), (3-aminopropyl) methyldiethoxysilane (APDES, 97%, Gelest), 3-cyanopropyltrichlorosilane (silane-CN, 97%, Sigma-Aldrich), (3-mercaptopropyl)triethoxysilane (silane-SH, 95%, Sigma-Aldrich),

and 3-(trimethoxysilyl)propylmethacrylate (Silane-C═O, 98%, Sigma Aldrich). Trimethylaluminum (TMA, 98%) was purchased from Strem Chemicals, Inc and HPLC grade water used for the ALD depositions was purchased from Sigma Aldrich. The ZrO_2 nanoparticles (~20 nm of diameter, U.S. Research Nanomaterials) and the commercial grids (Fotofab Inc.) were used for the FTIR study. Vapor phase reactions were conducted under ultrahigh pure N_2 (UHP, 99.999%) flow.

B. Atomic layer deposition and vapor-phase silane reactions

The Al_2O_3 ALD and subsequent vapor phase silane reactions were performed in a custom-made viscous flow hot-wall ALD reactor[31] using UHP N_2 carrier gas at a flow rate of 225 SCCM and a pressure of 1.1–1.2 Torr. The ALD Al_2O_3 used alternating exposures to TMA and H_2O at temperatures of 100, 150, and 200 °C using 1 s precursor exposures and 10 s N_2 purge periods between exposures (1 s:10 s:1 s:10 s). The TMA and H_2O were maintained at room temperature. The silanization reactions were performed immediately following the Al_2O_3 ALD at the same temperature, pressure, and flow conditions using multiple, 5 s silane exposures separated by 60 s of N_2 purging (5 s:60 s). The silane compounds were heated to 100 °C in stainless-steel containers to achieve a partial pressure of ~ 0.02–0.05 Torr in the ALD reactor during the silane exposures. The silane compound gas lines were also heated to 100 °C to avoid condensation.

C. Characterization

A Nicolet 6700 FTIR (Thermo Scientific) spectrometer was used to perform *in situ* FTIR measurements which was attached to a separate ALD reactor dedicated to FTIR studies equipped with IR-transparent KBr windows protected by gate valves during the chemical exposures.[32] The FTIR spectra were acquired by averaging 256 scans in the spectral range of 4000–750 cm^{-1}. The FTIR samples were prepared on a stainless-steel grid (50 μm thick, 50 μm bars with 200 μm spacing, Fotofab, Inc.) by pressing ZrO_2 nanoparticles (20 nm, U.S. Research Nanomaterials, Inc.) into the grid. The pressed ZrO_2 nanoparticle sample was loaded into the FTIR ALD reactor and allowed to equilibrate and outgas for 20 min at 100, 150, or 200 °C under 1 Torr of flowing N_2. Next, the ZrO_2 surface was coated with 20 cycles of ALD Al_2O_3 to fully cover the underlying ZrO_2 substrate and prepare a consistent, hydroxyl-terminated Al_2O_3 surface for the subsequent silane reactions.

A Thermo Fisher K-Alpha+ spectrometer was used to perform XPS measurements. All the XPS data were analyzed using Avantage software (Thermo Fisher), and the collected spectra were referenced to the 284.8 eV (adventitious C1s peak). An average of five scans was presented for each reported spectrum. The microfocused monochromatic Al Kα (1487 eV) x-ray beam was selected as the x-ray source with a spot size of 400 μm. When performing survey scans, 200.0 eV with a step size of 1.000 eV of pass energy was used. For the high-resolution XPS measurements, 50.0 eV with a step size of 0.100 eV of pass energy was used.

The hydrophilicity of the surfaces was determined by measuring the contact angle of a sessile water drop (10 μl) on thin film coatings prepared on polished silicon coupons using a contact angle goniometer (ramé-hart, model: 90 Pro, NJ, USA). To improve accuracy, five measurements were made at random locations on the sample and the average value was reported. The surface free energy was calculated using the Young–Dupre equation[33]

$$\Delta G_{SL} = (1 + \cos\theta)\gamma_L^T,$$

where θ is the measured water contact angle (deg.) and γ_L^T is the surface tension of water, 72.8 mJ m^{-2}

Atomic force microscopy (AFM) was conducted using an Asylum Research Cypher S AFM. High-speed, tapping-mode imaging was performed with gold-coated Asylum Research FS1500-AuD cantilevers having a resonance frequency of 1.5 MHz. Images were collected at room temperature and used a 500 or 800 mV set point. The set point value was selected to prevent tip-induced sample damage while maintaining sufficient imaging quality. A first-order flattening procedure in both the height and phase channels was used to process the AFM data. AFM samples were prepared using 200 Al_2O_3 ALD cycles on Si(100) coupons (~3 × 3 cm), followed by the silanization reaction.

Scanning electron microscopy (SEM) was performed using a field emission scanning electron microscope (FESEM, Hitachi S-4700-II) in an ultra-high-resolution mode at an accelerating voltage of 5.0 kV. For these measurements, the samples were mounted on metallic stubs and coated with ~ 8.0 nm gold to reduce sample charging.

III. RESULTS AND DISCUSSION

A. Reactivity of aminosilanes with ALD Al_2O_3

Aminosilanes such as 3-aminopropyltriethoxysilane (APTES) are commonly used to graft functional silanes to metal oxide substrates.[5,6,21] The APTES ethoxide groups react with surface hydroxyls through condensation reactions and the amine group can be used to selectively bind heavy metal ions such as copper and lead, or as a reactive handle for the subsequent functionalization with other compounds.[8,10,19] Previously, we reported the monolayer grafting of APTES on ALD Al_2O_3, ZnO, and TiO_2 surfaces.[30] In this previous study, we found that APTES reacts with hydroxylated Al_2O_3 via one- and two-anchored siloxy bonding at 100 °C, and two- and three-anchored siloxy bonding at 200 °C. In this work, we studied the vapor-phase reaction of aminosilanes with one ethoxy group, 3-aminopropylmonoethoxydimethylsilane (APMES), and two ethoxy groups, 3-aminopropyldiethoxymethylsilane (APDES) with ALD Al_2O_3 using *in situ* FTIR. Silanization was performed by dosing the silane compound 10 times using a 5 s dose and 60 s nitrogen purging (10 × 5 s:60 s) and FTIR spectra were recorded after each silane exposure. For both APMES and APDES, no changes were observed in the FTIR spectra after the third silane exposure indicating saturation of the silane reactions and ~ 90% of the saturated value was achieved after the first silane exposure suggesting rapid surface reactions.

APMES can only bond through a single ethoxide group as illustrated in Fig. 2(a). *In situ* FTIR difference spectra recorded following APMES adsorption at 150°C are presented in Fig. 2(b). To highlight the spectral changes associated with the silane reactions, the FTIR spectrum from the Al_2O_3 starting surface was subtracted

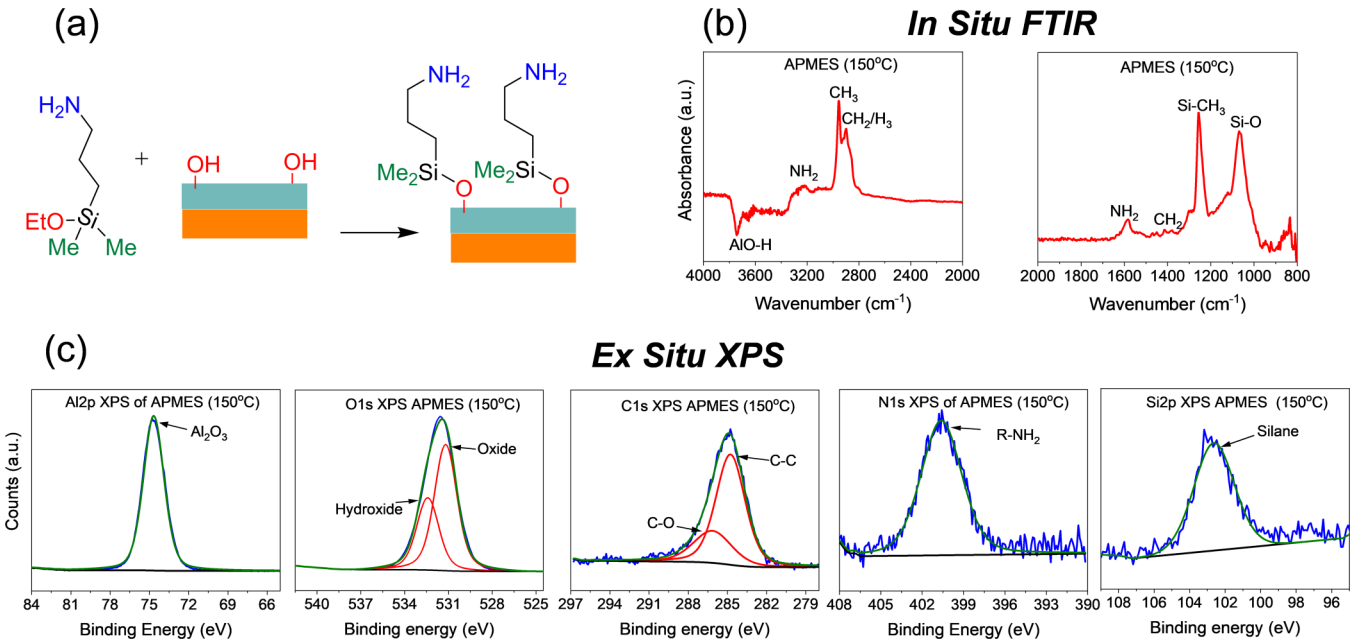

FIG. 2. 3-aminopropylmonoethoxydimethylsilane (APMES) reaction on ALD Al_2O_3. (a) Schematic description for APMES reaction. (b) *In situ* FTIR difference spectra following APMES reaction on Al_2O_3 at 150 °C referenced to the bare Al_2O_3 surface. (c) *Ex situ* high-resolution XPS spectra of APMES modified Al_2O_3 at 150 °C.

to obtain the difference spectrum. Consequently, negative spectral features indicate species consumed during the reaction and positive features indicate newly formed species. In Fig. 2(b), we observe a negative hydroxyl (—OH) stretching band at 3740 cm^{-1} consistent with the consumption of Al_2O_3 surface hydroxyls. The formation of aminosilane species is indicated by positive peaks for N—H stretching (3235 cm^{-1}), —NH_2 bending (1580 cm^{-1}), C—H stretching (2800–2900 cm^{-1}) and CH_2 bending at 1400 cm^{-1}, Si—CH_3 rocking (1255 cm^{-1}), and Si—O stretching (1000–1200 cm^{-1}). These spectral changes are in agreement with previous reports[30,34] and demonstrate the grafting of APMES to the ALD Al_2O_3 surface through condensation reactions. Figure 2(c) presents high-resolution XPS measurements of the APMES grafted samples. We observed signals for alkyl amine N1s at 400.5 eV and a siloxy Si2p peak at 102.5 eV, as well as the Al_2O_3 Al2p peak at 74.6 eV and O1s peaks at 531 eV and 532 eV. These XPS signals support the expected aminosilane chemical structure.

Next, we examined the reaction of diethoxy APDES with ALD Al_2O_3. APDES can react through either one or two ethoxy groups making it more complex than the monoethoxy APMES [Fig. 3(a)]. As expected, the *in situ* FTIR spectra recorded following the APDES reaction [Fig. 3(b)] are similar to those following the APMES reaction [Fig. 2(b)]. Negative OH peaks at 3740 cm^{-1} evidence the consumption of Al_2O_3 surface OH groups, and the formation of N—H stretching at 3235 cm^{-1}, —NH_2 bending at 1580 cm^{-1}, C—H stretching at 2800–2900 cm^{-1} and CH_2 bending at 1400 cm^{-1}, Si—CH_3 rocking (1255 cm^{-1}), and Si—O stretching (1000–1200 cm^{-1}) bands and demonstrate the successful bonding of APDES to the Al_2O_3 surface. A close inspection of the FTIR spectra reveals differences in the peak intensities following grafting of the APDES and APMES. For instance, the APDES grafted surface has a weaker methyl C—H stretching at 2960 cm^{-1}, and weaker Si—CH_3 rocking bands compared to the APMES. In addition, the APDES grafted surface features a distinct C—O stretching band at 1100 cm^{-1} due to unreacted ethoxides as compared to the APMES. XPS spectra of the APDES grafted surface [Fig. 3(c)] exhibit N1s (400.5 eV) and Si2p (102.5 eV) peaks similar to APMES indicating a similar chemical structure. The C1s spectrum also showed characteristic C═O peaks at ~290 eV, probably due to adventitious carbon introduced during sample transfer after the deposition. This is because we did not observe characteristic C═O stretching peaks around 1600–1900 cm^{-1} during the *in situ* FTIR measurements where there is no contamination.[35]

In our previous work examining (3-aminopropyl)triethoxysilane (APTES) grafting on ALD oxides, we calculated the surface density of grafted APTES molecules based on *in situ* FTIR and quartz crystal microbalance measurements combined with *ex situ* XPS measurements.[30] Here, we estimated the surface density of APMES and APDES by comparing the intensities of the high-resolution N1s XPS for the three aminosilane molecules. Figure 4(a) shows the surface density for grafted APMES, APDES, and APTES following reaction with ALD Al_2O_3 at 100 and 200 °C. It is interesting that we do not observe a monotonic change in the grafting density with number of ethoxy groups as might be expected if the value depended only on the number of ethoxy groups. Instead, the grafting density decreases between APMES and APDES, and then increases between APDES and APTES. The surface density of the grafted silanes can be rationalized by considering three factors: the reactivity of the siloxy Si—OEt bond [Fig. 4(b)], the steric effect

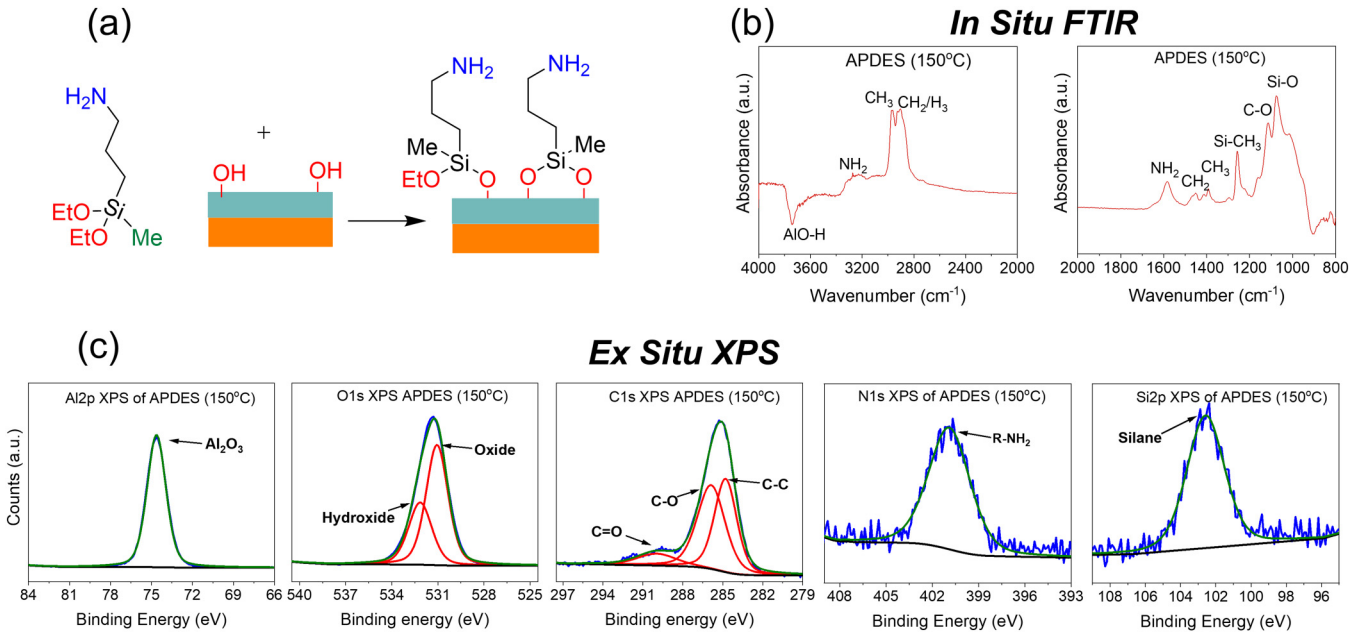

FIG. 3. 3-aminopropyldiethoxymethylsilane (APDES) reaction on ALD Al_2O_3. (a) Schematic description for APDES reaction. (b) *In situ* FTIR difference spectra following APDES reaction on Al_2O_3 at 150 °C reference to the bare Al_2O_3 surface. (c) *Ex situ* high-resolution XPS spectra of APDES modified Al_2O_3 at 150 °C.

of the ethoxy silanes [Fig. 4(c)] and the stochiometric ratio for the reaction of the silane with surface hydroxyls. Although triethoxy APTES should possess the highest Si—O reactivity due to the combined electron withdrawing effects of the three oxygens, APTES has a 0.33:1 stochiometric ratio of aminosilane/hydroxyl which may lead to unreacted ethoxides, and the unreacted ethoxides will have a higher steric effect compared to methyl groups. Consequently, APTES showed moderate reactivity as compared to other aminosilanes. On the other hand, despite the low expected Si—O reactivity, APMES exhibits the highest grafting density due to the low steric hindrance of the methyl groups and 1:1 stochiometric ratio with surface OH groups. At the higher temperature of 200 °C, the surface density of APTES and APDES decreased slightly. We attribute this to the reduced OH coverage on the Al_2O_3 surface and higher aminosilane:OH stoichiometric ratio (i.e., less residual ethoxy groups) compared to the 100 °C reaction based on our previous study.[30] APMES showed a slightly higher surface density at 200 °C compared to 100 °C. Unlike APTES and APDES, monoethoxy APMES can only react through a 1:1 stoichiometry at both 100 °C and 200 °C, and the slightly higher coverage at 200 °C may reflect a faster condensation reaction producing a more saturated surface.

To examine the effects of the aminosilane grafting density and residual ligands on the surface properties, SEM, AFM, and WCA measurements were conducted on these surfaces. SEM images of bare Al_2O_3 and the three aminosilane-grafted Al_2O_3 surfaces all exhibited a featureless morphology with no evidence of agglomerates that are sometimes produced during liquid-phase grafting[36] (see the supplementary material[37] for SEM images). Figure 5(a) shows AFM images and RMS surface roughness values for the ALD Al_2O_3 and the three aminosilane treated Al_2O_3 surfaces. The vapor phase aminosilane grafting yielded smooth films with low RMS surface roughness values of 0.24 nm for APTES, 0.34 nm for APDES and 0.54 nm for APMES, all of which are similar to the RMS roughness value of 0.32 nm for the bare ALD Al_2O_3 substrate. The SEM and AFM measurements indicate a smooth and uniform aminosilane coating on the ALD Al_2O_3 substrate. A similar study of aminosilane grafting on thermally grown SiO_2[36] reported RMS roughness values of 0.22 nm for APTES, 0.19 nm for APDES and 0.18 nm for APMES following vapor-phase grafting that were similar to the 0.45 nm roughness of the SiO_2 substrate. In contrast, solution-phase grating of aminosilanes yielded RMS roughness values as high as 20 nm due to severe agglomeration under some conditions.

Next, we performed WCA measurements on the substrate silicon wafer with native SiO_2 layer, ALD Al_2O_3 coated silicon, and aminosilane-grafted surfaces and the results are presented in Fig. 5(b). To avoid contamination of the surfaces from ambient exposure, the WCA measurements were conducted immediately after the deposition (~5 min). Compared to the native oxide on the silicon wafer which exhibited a WCA of $\theta = 24°$, the ALD Al_2O_3 surface was more hydrophilic and showed θ=13°. Following grafting of the aminosilanes, the WCA increased to $\theta = 37°$ for APTES, $\theta = 42°$ for APDES, and $\theta = 63°$ for APMES, indicating greater hydrophobicity when the Al_2O_3 hydroxyls are replaced with organic species. Similarly, the surface free energy (SFE) decreased from 131 mJ/m^2 for APTES to 127 mJ/m^2 for APDES and 106 mJ/m^2 for APMES. Comparing the WCA and SFE values for the different aminosilanes, it appears that the surfaces become more hydrophobic as

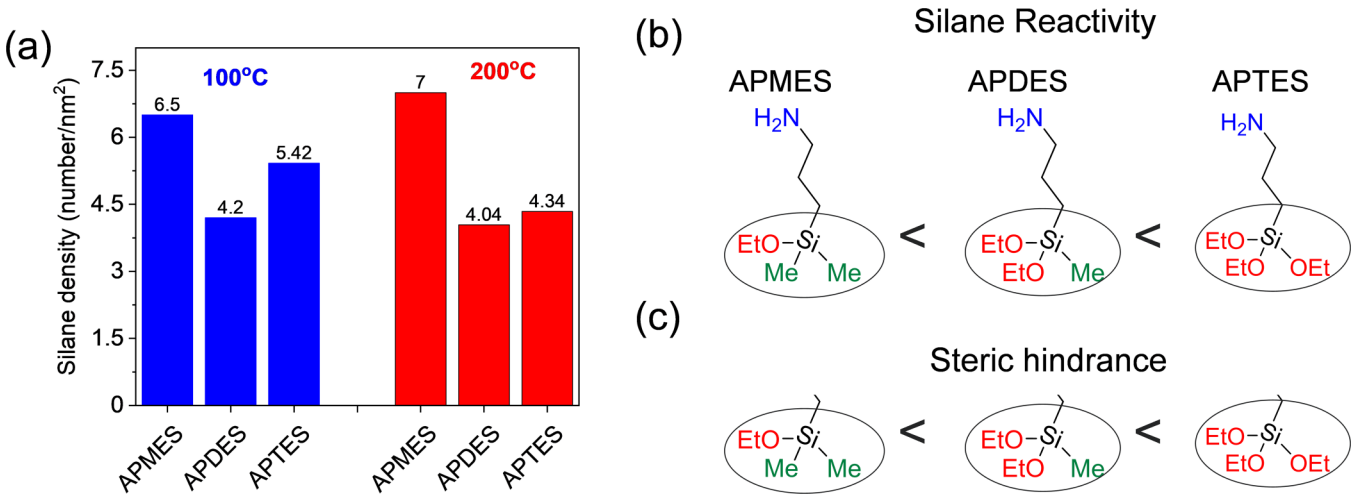

FIG. 4. (a) Surface density of grafted aminosilanes on ALD Al_2O_3. (b) Reactivity comparison of aminosilanes. (c) Steric hindrance effects of aminosilanes.

the number of methyl groups increases [Fig. 5(c)]. These observations are similar to the work of Yadav *et al.* which reported θ = 40° for APTES, θ = 54° for APDES and θ = 60° for APMES on thermally grown SiO_2.[36] However, much higher hydrophobicity with contact angles of 115°–135° were reported for solution-phase functionalization of powders and membranes using longer chain octyl silanes.[15–17] Hydrophobicity and WCA depend on factors including surface chemistry, surface roughness and surface density of adsorbed species.[15] In our work, due to the hydrophilic amines, smaller three-carbon chain, ultrasmooth silicon substrates, and lower surface density, a lower hydrophobicity is observed. However, if this functionalization is applied to membranes and powders, we believe that higher hydrophobicity could be achieved due to the higher surface roughness of membranes and powders.

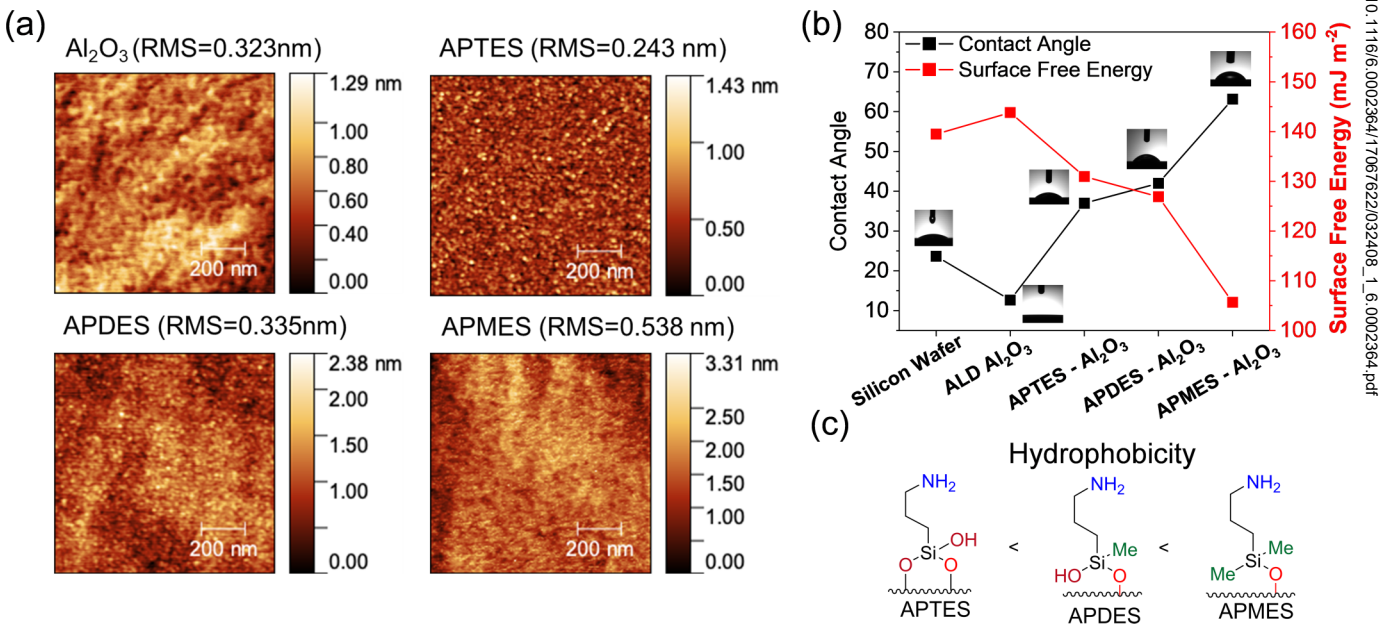

FIG. 5. (a) AFM images with RMS surface roughness values, (b) WCA measurements and surface free energy calculations of ALD Al_2O_3, APTES, APDES, and APMES coated on ALD Al_2O_3 at 150 °C. (c) Hydrophobicity comparison of different aminosilanes.

B. Reactivity of thiol-, ester-, and cyanosilanes with ALD Al_2O_3

We next examined the reaction of the thiol terminated 3-mercaptopropyltriethoxysilane (silane-SH) with ALD Al_2O_3 as depicted in Fig. 6(a). *In situ* FTIR spectra were recorded after each silane-SH exposure (5 s Silane-SH: 60 s N_2). No further changes were observed in the spectra after 5–6 silane exposures at 150°C indicating saturation of the silane reaction with the Al_2O_3 surface, and the FTIR absorption intensity achieved ~60% of the saturated value after the first silane exposure. These findings suggest that the Silane-SH reacts more slowly with the hydroxylated ALD Al_2O_3 surface compared to the aminosilanes. The FTIR difference spectrum recorded after the saturation Silane-SH exposure is presented in Fig. 6(b) and exhibits negative OH peaks at 3740 cm^{-1} showing the consumption of Al_2O_3 surface hydroxyls, and the formation of C—H stretching at 2800–2900 cm^{-1} and CH_2 bending at 1400 cm^{-1}, and Si—O stretching (1000–1200 cm^{-1}) bands demonstrating the successful bonding of silane-SH to the surface. However, the S—H stretching feature expected at ~2500 cm^{-1} was not detected in the FTIR measurements. The S—H stretching feature is weak, and we speculate that IR absorption from S—H in the grafted monolayer is below our detection limit. This is in line with previous FTIR studies of S—H containing species.[38,39] Figure 6(c) shows high-resolution XPS measurements of the Silane-SH surface and reveals the Al2p peak at 74.6 eV, and O1s peaks at 531 eV and 532 eV characteristic of Al_2O_3.[30,40] The Si2p peak at 102 eV and S2p peak at 164 eV are similar to previously reported values[41,42] and indicate the grafting of silane-SH to the ALD Al_2O_3 surface. The absence of sulfide S2p peaks at 161–162 eV indicates that silane-SH only reacts through the ethoxy groups and not through the terminal —SH group. Our XPS measurements found a lower sulfur S2p content (1.02–1.05 at. %) compared to Si2p (1.45–1.70 at. %) at grafting temperatures of 100, 150, and 200°C (Table S1 in the supplementary material),[37] and we attribute this discrepancy to x-ray induced damage of the monolayer thiol.[43] During our investigation, we found that monolayer thiols are oxidized to sulfonic acids when heated to 100, 150, and 200 °C under air as evidenced by the formation of sulfonic acid S2p peaks at 169 eV (see supplementary material[37] for surface oxidation of thiols). Therefore, to avoid oxidation, the ALD reactor was cooled below 50 °C before removing the silane-SH samples.

Among the five silanes studied here, only the vapor-phase grafting of the ester-based (3-trimethoxysilyl)propylmethacrylate (silane-C═O) was unsuccessful. *In situ* FTIR measurements revealed no reaction of silane-C═O on ALD Al_2O_3 under the vapor-phase reaction conditions at 100 °C (see supplementary materials[37] for silane-C═O reaction). When the temperature was increased to 150 °C, strong Si—O and C—O peaks emerged at 800–1200 cm^{-1}, but no carbonyl peaks were observed at 1600–1800 cm^{-1}. We attribute these changes to the decomposition of Silane-C═O at 150 °C directly on the Al_2O_3 surface or elsewhere within the ALD reactor followed by adsorption of the degradation products on the Al_2O_3.

Finally, to investigate the behavior of chlorosilanes in vapor-phase grafting, we examined the reaction of (3-cyanopropyl)trichlorosilane (silane-CN) with ALD Al_2O_3 at different temperatures.

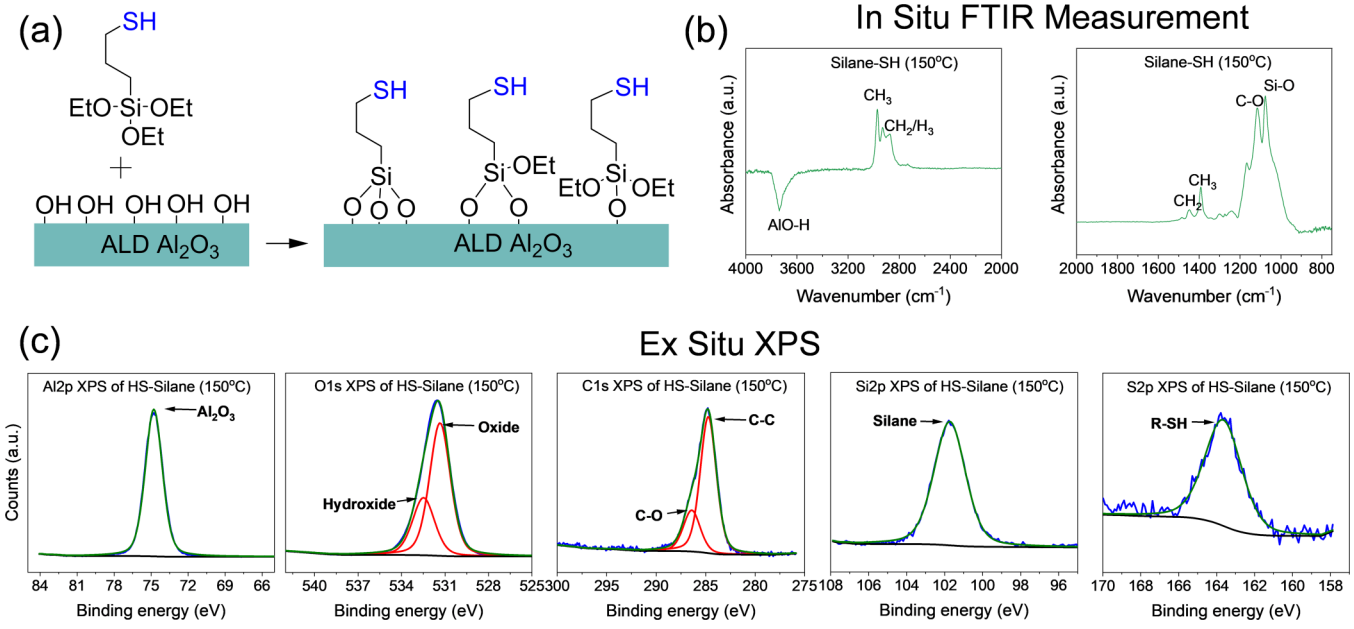

FIG. 6. Reaction of 3-mercaptopropyltriethoxysilane (silane-SH) with ALD Al_2O_3. (a) Schematic description of silane-SH reaction. (b) *In situ* FTIR difference spectra of Silane-SH reaction on ALD Al_2O_3 at 150 °C referenced to the bare Al_2O_3 surface. (c) *Ex situ* high-resolution XPS spectra of silane-SH modified Al_2O_3 prepared at 150 °C.

Chlorosilanes react with hydroxyl groups similar to ethoxides but release HCl as the by-product [Fig. 7(a)]. *In situ* FTIR spectra were recorded after each silane-CN exposure (5 s silane-CN: 60 s N_2). Analysis of these spectra revealed that 8–9 silane-CN exposures were required to saturate the reaction and the first silane-CN produced 62% saturation. These findings suggest that the chlorosilane reacts more slowly compared to the ethoxy-based aminosilanes and silane-SH. Figure 7(b) shows the FTIR difference spectrum following a saturating silane-CN exposure on the hydroxylated ALD Al_2O_3 surface. The formation of Si—O stretching bands at 950–1200 cm^{-1}, CH_2 bending bands at ~1400 cm^{-1}, C—H stretching bands at 2800–3000 cm^{-1}, nitrile stretching bands at ~2330 cm^{-1}, and the consumption of O—H stretching bands at ~3700 cm^{-1} confirm the grafting of silane-CN to the ALD Al_2O_3. *Ex situ* XPS measurements [Fig. 7(d)] are consistent with a nitrile-based silane grafted to the surface. The silane Si2p peak at 102 eV and nitrile N1s peak at 400 eV are in agreement with reported nitrile-based silane structures.[44,45] The C1s spectra of the surface also revealed adventitious carbon peaks due to contamination during sample transfer. *Ex situ* XPS measurements indicate ~1% Cl on the surface following grafting of the Silane-CN (see supplementary materials[37] for elemental composition of films), and the FTIR data also revealed that HCl binds to the nitriles and surface hydroxyls [Fig. 7(c)]. These findings may explain the relatively slow reaction of the chlorosilane-based silane-CN since the adsorbed HCl may block potential grafting sites. A broad peak at ~3500 cm^{-1} can be assigned to bound HCl and a peak at 2250 cm^{-1} suggests that H—Cl also binds to nitriles. The intensity of the broad HCl band and the nitrile shoulder peak decrease when the grafting temperature increases from 100 to 150 °C and 200 °C [Fig. 7(c)]. We attribute this to a lower concentration of physisorbed HCl at higher substrate temperatures based on the thermodynamics of surface adsorption.[46,47]

By using the elemental content from high-resolution N1s and S2p XPS spectra, the reacted amount of three different silanes were compared at 100 and 200 °C. The reactivity difference of silanes

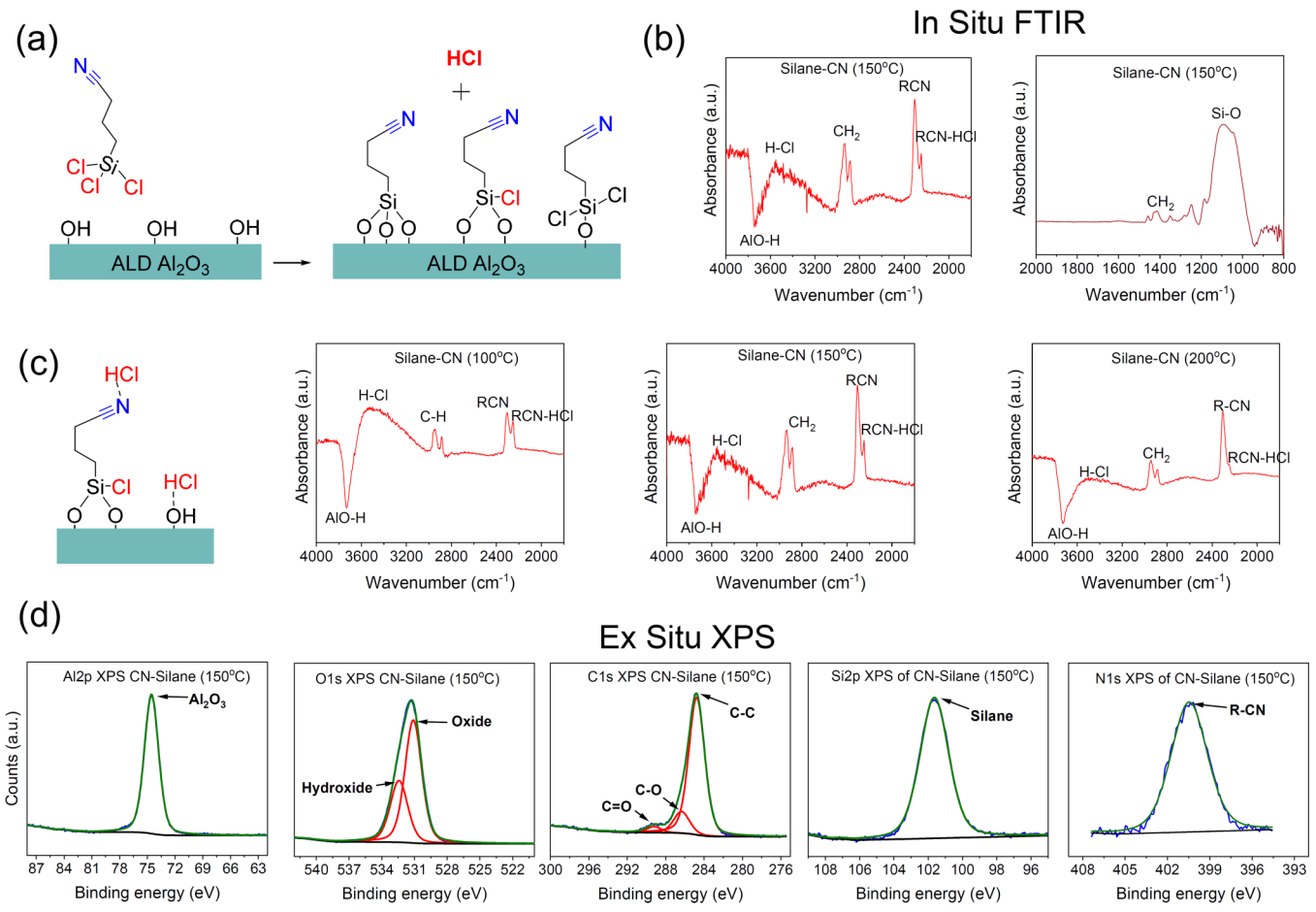

FIG. 7. 3-cyanopropyltrichlorosilane (silane-CN) reaction on ALD Al_2O_3. (a) Schematic illustration of the silane-CN reaction. (b) *In situ* FTIR difference spectra following silane-CN grafting on Al_2O_3 at 100, 150, and 200 °C referenced to the bare Al_2O_3 surface. (c) Schematic of HCl binding to surface OH and silane C-N groups following silane-CN reaction on ALD Al_2O_3. (d) *Ex situ* high-resolution XPS spectra following silane-CN grafting on Al_2O_3 at 150 °C.

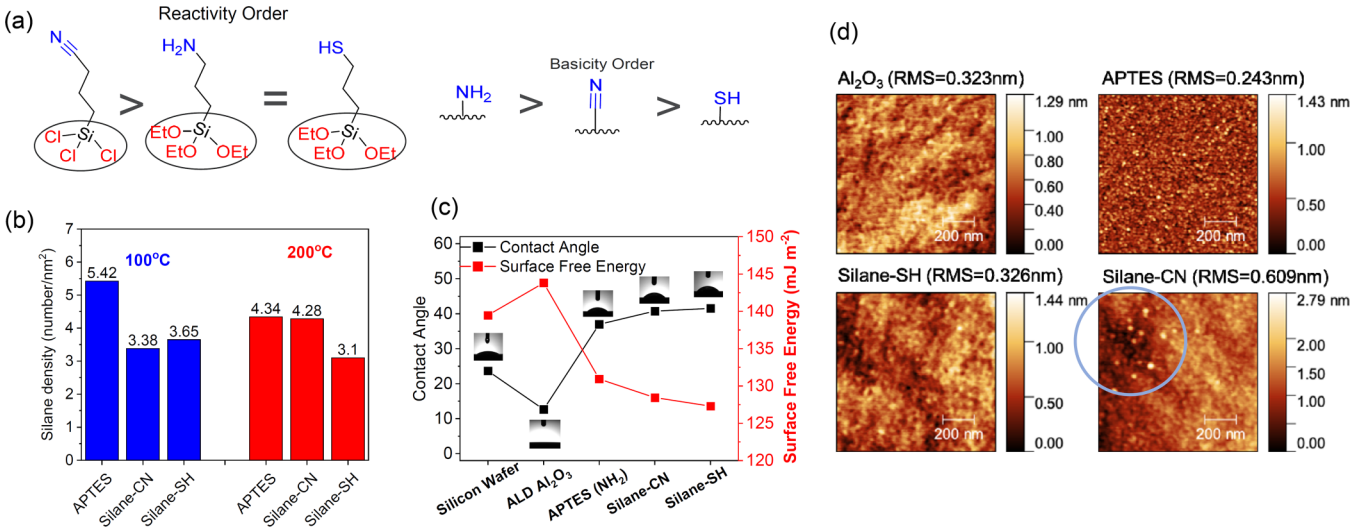

FIG. 8. (a) Reactivity comparison of ethoxy- and chlorosilanes, and the basicity comparison of functional silanes. (b) Silane density on ALD Al_2O_3. (c) WCA measurements and surface free energy calculations. (d) AFM images of ALD Al_2O_3, and APTES, silane-SH and silane-CN coated Al_2O_3 prepared at 150 °C.

will be dictated by the reactivity of the silyl ligand (i.e., Si—O versus Si—Cl bonding) and the basicity of the functional moiety (X = —NH_2, —CN, —SH) [Fig. 8(a)]. As presented in Fig. 8(b), although Si—Cl has a higher reactivity than Si—OEt toward hydroxyls in most cases, APTES showed the highest surface density as a result of the amine group which acts as a catalyzing agent.[37,48] At the higher reaction temperature of 200 °C, the surface density of grafted silane species decreased for APTES and silane-SH due to the reduced hydroxyl density at the higher temperature. In contrast, the surface density of the chlorosilane increased at the higher grafting temperature. It may be that the HCl by-product adsorbs more strongly to surface hydroxyls at the lower temperature and blocks potential adsorption sites for the chlorosilane. Alternatively, HCl may reduce the nucleophilicity of the surface hydroxyls leading to a slower grafting reaction at the lower temperature. To compare the surface hydrophobicity of these functional silanes, WCA measurements were performed, and the results are presented in Fig. 8(c). To avoid air contamination, the samples were tested immediately after (~5 min) preparation. All three silanes showed a significantly larger WCA after grafting compared to the bare Al_2O_3 substrate from θ = 13° (Al_2O_3) to θ = 37° (APTES), θ = 41° (silane-CN), and θ = 42° (silane-SH). Similarly, the SFE decreased from 131 mJ/m^2 for APTES to 128 mJ/m^2 for silane-CN and 127 mJ/m^2 for silane-SH. We suspect that the lower WCA and higher SFE for APTES compared to the other silanes results from the hydrophilic amine group. To investigate the surface properties of these silanes, SEM AFM measurements were performed. The SEM images did not show any agglomerates or irregular morphology indicating uniform coatings of the silanes (see supplementary material[37] for SEM images). AFM images and RMS surface roughness calculations of these silane coated Al_2O_3 surfaces are presented in Fig. 8(d). The ethoxy-based silanes, APTES and silane-SH, show a morphology and RMS surface roughness (0.243 nm for APTES and 0.326 nm for silane-SH) that are similar to the bare ALD Al_2O_3 surface, indicating uniform monolayer film formation. However, AFM images of the chlorosilane-based silane-CN showed agglomerates with lateral dimensions of 10–35 nm and a height of 2–3 nm in some regions and a higher RMS roughness (0.609 nm). It may be that the adsorbed HCl by-product nucleates the formation of multilayer agglomerates.

IV. SUMMARY AND CONCLUSIONS

In conclusion, we have reported the vapor-phase synthesis of five different silanes with various functionality on the surface of atomic layer deposited aluminum oxide. Nearly all of the silane compounds exhibited self-limiting surface chemistry via an exchange between the silane ligands and the Al_2O_3 hydroxyl groups. The exception was the silane-C═O that showed no reaction at 100°C and decomposed at 150 °C. The silane surface density following vapor-phase grafting was dictated by factors including the Al_2O_3 hydroxyl density, the chemical reactivity of the silane ligands, and steric effects. We found that methyl substituted aminosilanes such as APMES yielded more hydrophobic surfaces compared to their nonmethylated aminosilane counterparts. The chlorosilane compound, silane-CN, produced a nonuniform film that we attribute to binding of the HCl by-product. On the other hand, ethoxy-based silanes yielded smooth, uniform monolayer films. This study provides a detailed characterization of the vapor-phase grafting of silane compounds that we hope will assist in the design and manufacture of improved materials for water treatment.

ACKNOWLEDGMENTS

This work was supported as part of the Advanced Materials for Energy-Water Systems (AMEWS) Center, an Energy Frontier Research Center funded by the U.S. Department of Energy, Office

of Science, Basic Energy Sciences. J.G.M. and S.J.S. acknowledge support from an NSF Alliances for Graduate Education and Professoriate supplement to Grant No. CHE-1900188. AFM measurements were supported by the NSF-Materials Research Science and Engineering Center at the University of Chicago under Grant No. NSF-DMR-2011854.

AUTHOR DECLARATIONS

Conflict of Interest

The authors have no conflicts to disclose.

Author Contributions

Vepa Rozyyev: Data curation (lead); Investigation (lead); Writing – original draft (lead). **Rahul Shevate:** Data curation (supporting); Investigation (supporting). **Rajesh Pathak:** Data curation (supporting); Investigation (supporting). **Julia G. Murphy:** Data curation (supporting); Investigation (supporting); Writing – review & editing (equal). **Anil U. Mane:** Data curation (supporting); Investigation (supporting). **S. J. Sibener:** Writing – review & editing (supporting). **Jeffrey W. Elam:** Conceptualization (lead); Funding acquisition (lead); Writing – review & editing (lead).

DATA AVAILABILITY

The data that support the findings of this study are available within the article and its supplementary material.

REFERENCES

[1]J. Eliasson, Nature **517**, 6 (2015).
[2]M. A. Shannon, P. W. Bohn, M. Elimelech, J. G. Georgiadis, B. J. Mariñas, and A. M. Mayes, Nature **452**, 301 (2008).
[3]V. Krstić, T. Urošević, and B. Pešovski, Chem. Eng. Sci. **192**, 273 (2018).
[4]E. Barry *et al.*, Chem. Rev. **121**, 9450 (2021).
[5]S. P. Pujari, L. Scheres, A. T. M. Marcelis, and H. Zuilhof, Angew. Chem. Int. Ed. **53**, 6322 (2014).
[6]L. Wang, U. S. Schubert, and S. Hoeppener, Chem. Soc. Rev. **50**, 6507 (2021).
[7]M. Grandbois, M. Beyer, M. Rief, M. Clausen-Schaumann, and H. E. Gaub, Science **283**, 1727 (1999).
[8]J. You, L. Wang, Y. Zhao, and W. Bao, J. Clean. Prod. **281**, 124668 (2021).
[9]X. Zhuang, Q. Zhao, and Y. Wan, J. Mater. Chem. **20**, 4715 (2010).
[10]M. Karakoy, E. Gultepe, S. Pandey, M. A. Khashab, and D. H. Gracias, Appl. Surf. Sci. **311**, 684 (2014).
[11]Z. Wang, L. Scheres, H. Xia, and H. Zuilhof, Adv. Funct. Mater. **30**, 1908098 (2020).
[12]N. Bouazizi, J. Vieillard, B. Samir, and F. Le Derf, Polymers **14**, 378 (2022).
[13]F. Ahmadijokani, S. Ahmadipouya, H. Molavi, and M. Arjmand, Dalton Trans. **48**, 13555 (2019).
[14]H. Riazi, M. Anayee, K. Hantanasirisakul, A. A. Shamsabadi, B. Anasori, Y. Gogotsi, and M. Soroush, Adv. Mater. Interfaces **7**, 1902008 (2020).
[15]J. Kujawa, W. Kujawski, S. Cerneaux, G. Li, and S. Al-Gharabli, J. Membr. Sci. **596**, 117597 (2020).
[16]J. Kujawa, S. Al-Gharabli, W. Kujawski, and K. Knozowska, ACS Appl. Mater. Interfaces **9**, 6571 (2017).
[17]J. Kujawa and W. Kujawski, ACS Appl. Mater. Interfaces **8**, 7509 (2016).
[18]J. Kujawa, S. Cerneaux, W. Kujawski, and K. Knozowska, Appl. Sci. **7**, 402 (2017).
[19]F. Zhang, K. Sautter, A. M. Larsen, D. A. Findley, R. C. Davis, H. Samha, and M. R. Linford, Langmuir **26**, 14648 (2010).
[20]A. Y. Fadeev and T. J. McCarthy, Langmuir **15**, 3759 (1999).
[21]C. Haensch, S. Hoeppener, and U. S. Schubert, Chem. Soc. Rev. **39**, 2323 (2010).
[22]L. Wang, C. Shi, L. Wang, L. Pan, X. Zhang, and J.-J. Zou, Nanoscale **12**, 4790 (2020).
[23]V. B. Cashin, D. S. Eldridge, A. Yu, and D. Zhao, Environ. Sci. Water Res. Technol. **4**, 110 (2018).
[24]S. Sonal and B. K. Mishra, Chem. Eng. J. **424**, 130509 (2021).
[25]S. M. George, Chem. Rev. **110**, 111 (2010).
[26]V. Cremers, R. L. Puurunen, and J. Dendooven, Appl. Phys. Rev. **6**, 021302 (2019).
[27]R. W. Johnson, A. Hultqvist, and S. F. Bent, Mater. Today **17**, 236 (2014).
[28]R. L. Puurunen, J. Appl. Phys. **97**, 121301 (2005).
[29]M. Leskelä and M. Ritala, Angew. Chem. Int. Ed. **42**, 5548 (2003).
[30]V. Rozyyev, J. G. Murphy, E. Barry, A. U. Mane, S. J. Sibener, and J. W. Elam, Appl. Surf. Sci. **562**, 149996 (2021).
[31]J. W. Elam, M. D. Groner, and S. M. George, Rev. Sci. Instrum. **73**, 2981 (2002).
[32]D. J. Comstock and J. W. Elam, Chem. Mater. **24**, 4011 (2012).
[33]M. E. Schrader, Langmuir **11**, 3585 (1995).
[34]R. M. Pasternack, S. Rivillon Amy, and Y. J. Chabal, Langmuir **24**, 12963 (2008).
[35]B. Smith, Spectroscopy **37**, 16 (2022).
[36]A. R. Yadav, R. Sriram, J. A. Carter, and B. L. Miller, Mater. Sci. Eng. C **35**, 283 (2014).
[37]See supplemetary materials at https://www.scitation.org/doi/suppl/10.1116/6.0002364 for supporting figures of SEM images, surface thiol oxidation, XPS data, *in situ* FTIR data, and elemental composition of films.
[38]X. Meng, Y. Cao, J. A. Libera, and J. W. Elam, Chem. Mater. **29**, 9043 (2017).
[39]S. Sinha, N. Mahuli, and S. K. Sarkar, J. Vac. Sci. Technol. A **33**, 01A139 (2014).
[40]R. H. Temperton, A. Gibson, and J. N. O'Shea, Phys. Chem. Chem. Phys. **21**, 1393 (2019).
[41]B. Tao and C. Xian-Hua, Wear **261**, 730 (2006).
[42]F. Sinapi, T. Issakova, J. Delhalle, and Z. Mekhalif, Thin Solid Films **515**, 6833 (2007).
[43]D. Zerulla and T. Chassé, Langmuir **15**, 5285 (1999).
[44]Y. R. Park, H. Y. Jeong, Y. S. Seo, W. K. Choi, and Y. J. Hong, Sci. Rep. **7**, 46422 (2017).
[45]K. Kishi, Y. Okino, and Y. Fujimoto, Surf. Sci. **176**, 23 (1986).
[46]H. Swenson and N. P. Stadie, Langmuir **35**, 5409 (2019).
[47]K. S. W. Sing, Pure Appl. Chem. **57**, 603 (1985).
[48]L. D. White and C. P. Tripp, J. Colloid Interface Sci. **227**, 237 (2000).

Supplementary Materials

Vapor-phase grafting of functional silanes on atomic layer deposited Al_2O_3

Vepa Rozyyev[a,b,c], Rahul Shevate[b], Rajesh Pathak[b], Julia Murphy[c,d], Anil U. Mane[b,c], S. J. Sibener[c,d], Jeffrey W. Elam*[b,c]

a) Pritzker School of Molecular Engineering, The University of Chicago, 5640 S. Ellis Ave Chicago, IL 60637 USA

b) Applied Materials Division, Argonne National Laboratory, Lemont, IL 60439, USA

c) Advanced Materials for Energy-Water Systems (AMEWS) Energy Frontier Research Center (EFRC), Lemont, IL 60439, USA

d) The James Franck Institute and Department of Chemistry, The University of Chicago, 929 E. 57th Street, Chicago, IL 60637, USA

Electronic mail: jelam@anl.gov

I. SEM IMAGES OF SILANE GRAFTED Al_2O_3 SURFACES.

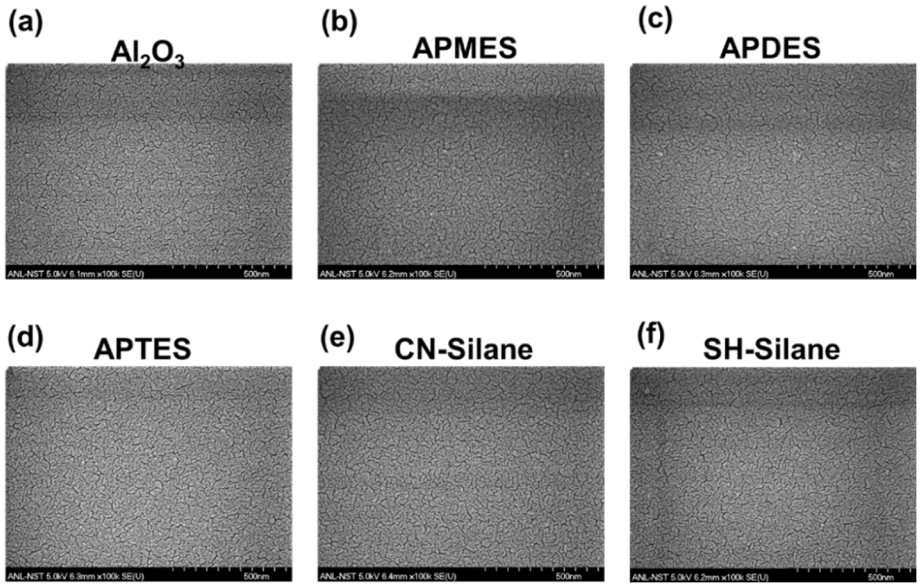

Figure S1. Scanning electron microscope (SEM) images of (a) 200 cycles ALD Al_2O_3, and Al_2O_3 functionalized with (b) APMES, (c) APDES, (d) APTES, (e) CN-Silane, and (f) SH-Silane at 150ºC.

II. SURFACE OXIDATION OF THIOLS

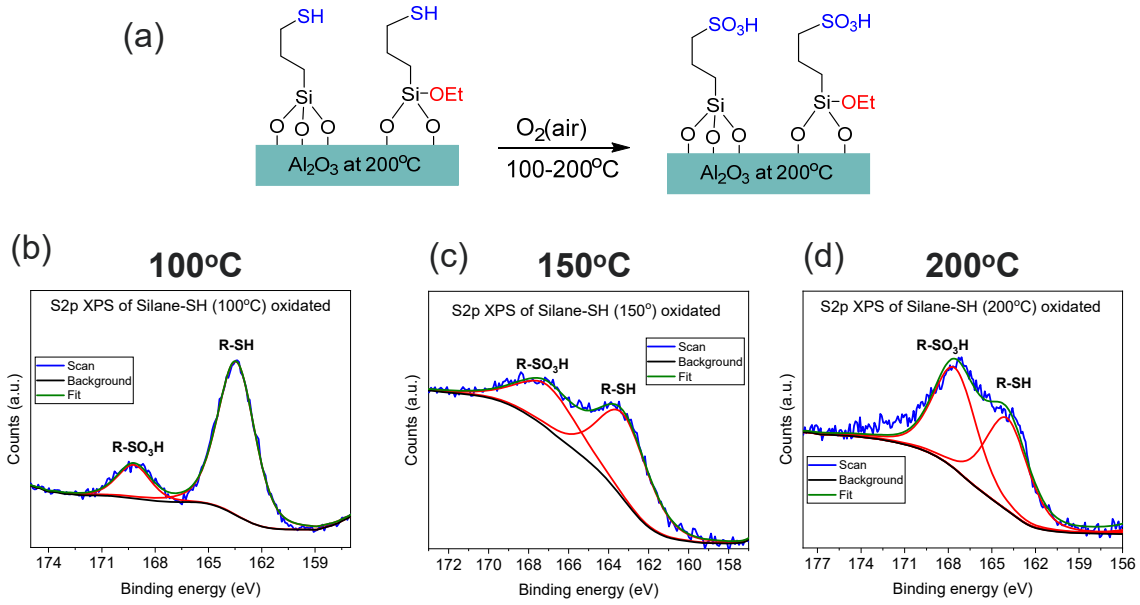

Figure S2. Oxidation of 3-mercaptopropyltriethoxysilane (Silane-SH) coated Al_2O_3 by air exposure. (a) Reaction scheme for thiol oxidation to form sulfonic acid and XPS S2p spectra of Silane-SH coated Al_2O_3 following air exposure at (b) 100 °C (c) 150 °C and (d) 200 °C.

III. SILANE-C=O REACTION

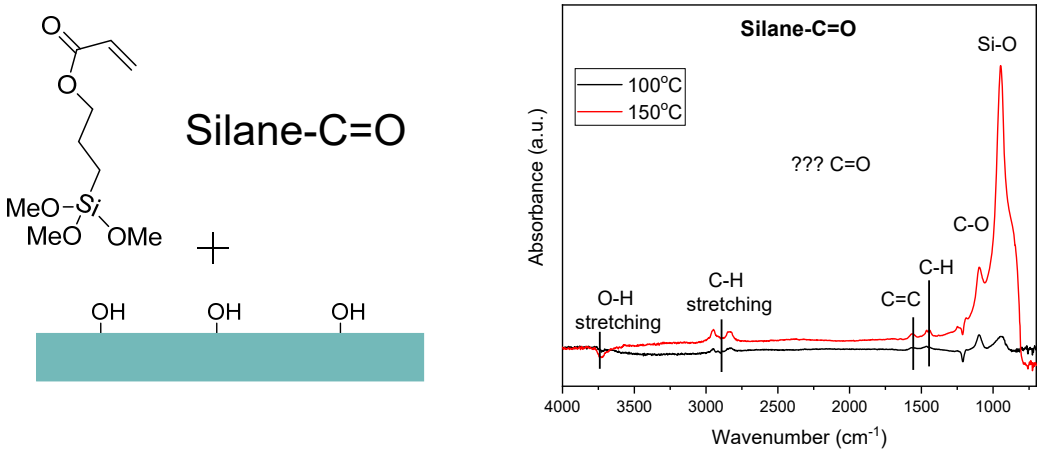

Figure S3. The reaction of 3-(trimethoxysilyl)propylmethacrylate (Silane-C=O) with ALD Al_2O_3 under vapor-phase reaction conditions at 100°C and 150°C.

IV. HCl BINDING TO NITRILES

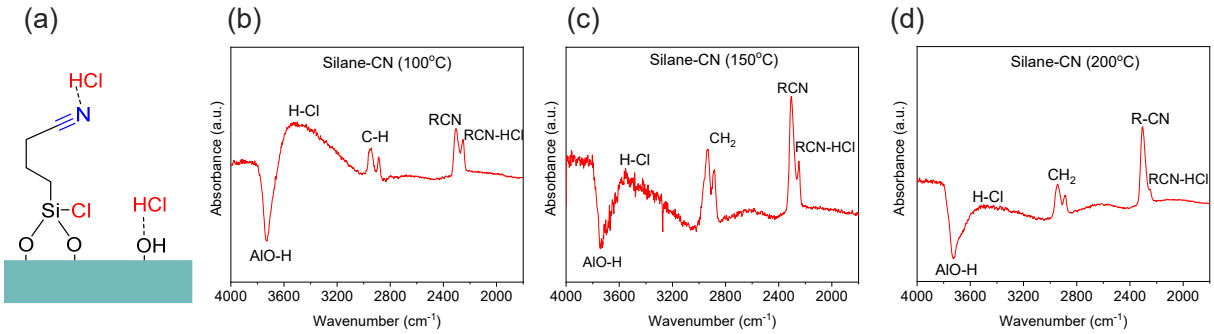

Figure S4. (a) Illustration of HCl binding to nitrile group of Silane-CN and surface hydroxyls on ALD Al_2O_3. FTIR spectra of Silane-CN grafted to ALD Al_2O_3 at (b) 100°C, (c) 150°C, and (d) 200°C.

V. XPS DATA OF SILANE GRAFTED SURFACES

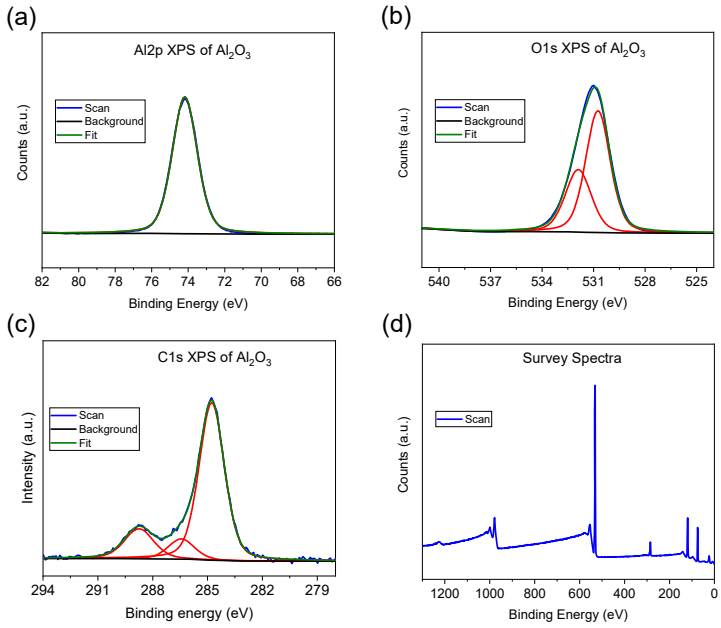

Figure S5. XPS spectra of Al_2O_3 prepared at 150°C using 200 ALD cycles of TMA/water. (a) Al2p, (b) O1s, (c) C1s, (d) Survey spectrum.

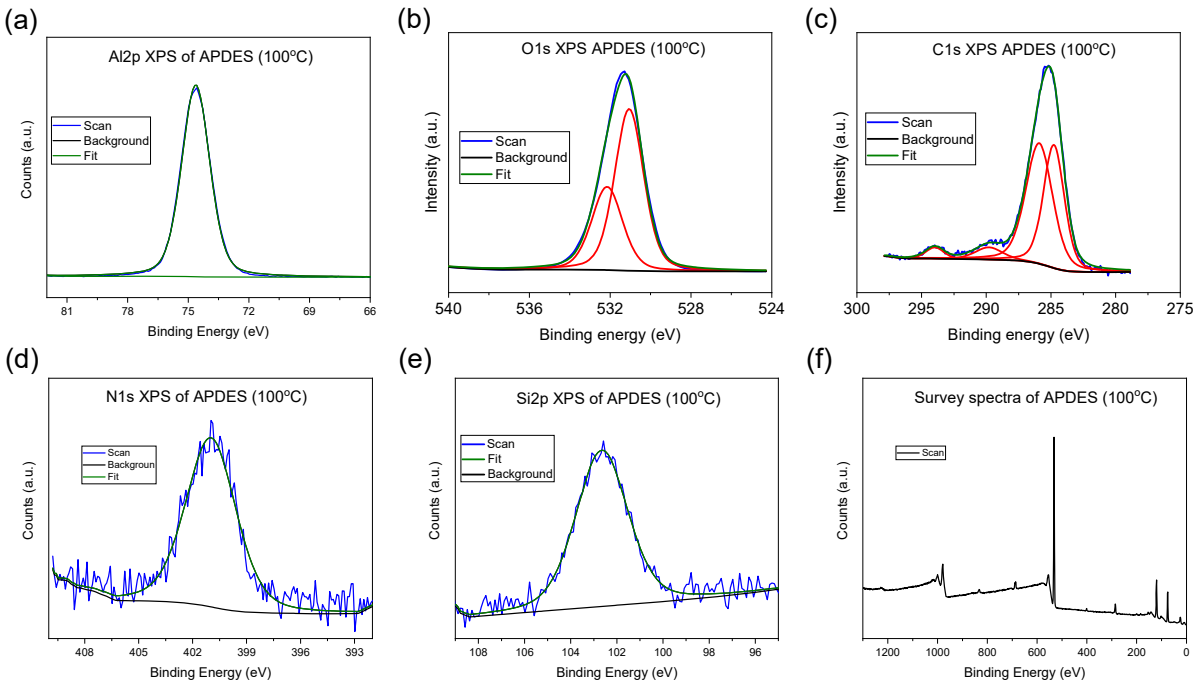

Figure S6. XPS spectra of 3-aminopropyldiethoxymethylsilane (APDES) coated Al_2O_3 prepared at 100°C. (a) Al2p, (b) O1s, (c) C1s, (d) N1s, (e) Si2p, (f) Survey spectrum.

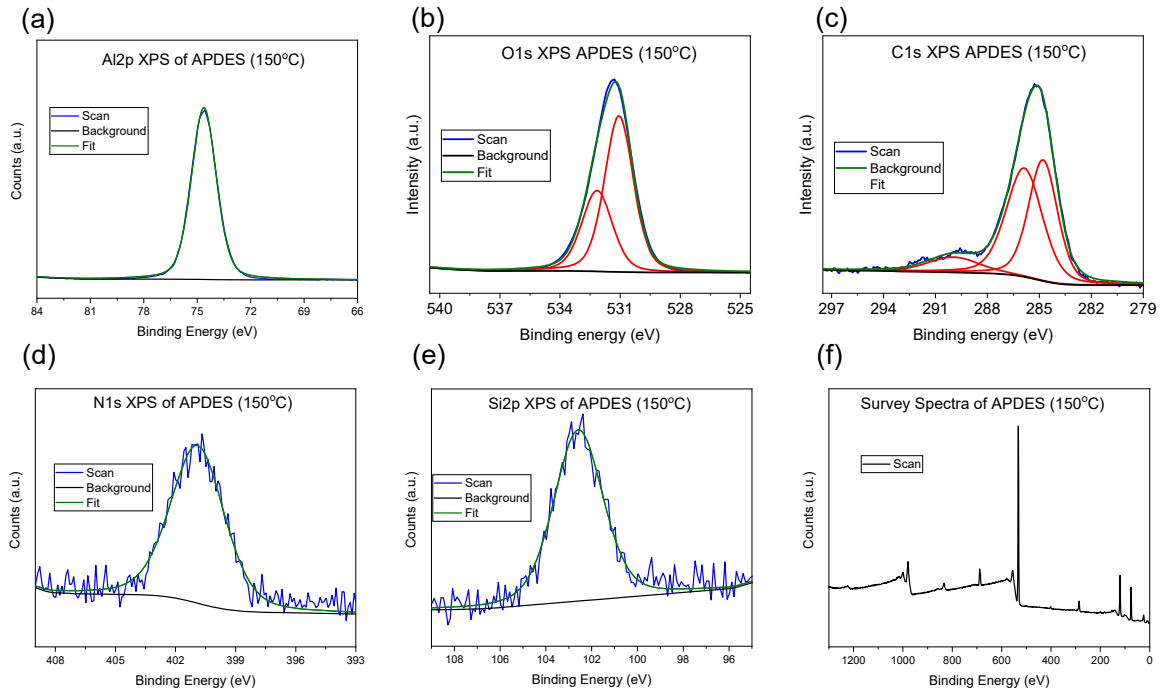

Figure S7. XPS spectra of 3-aminopropyldiethoxymethylsilane (APDES) grafted to ALD Al_2O_3 at 150°C. (a) Al2p, (b) O1s, (c) C1s, (d) N1s, (e) Si2p, (f) Survey spectrum.

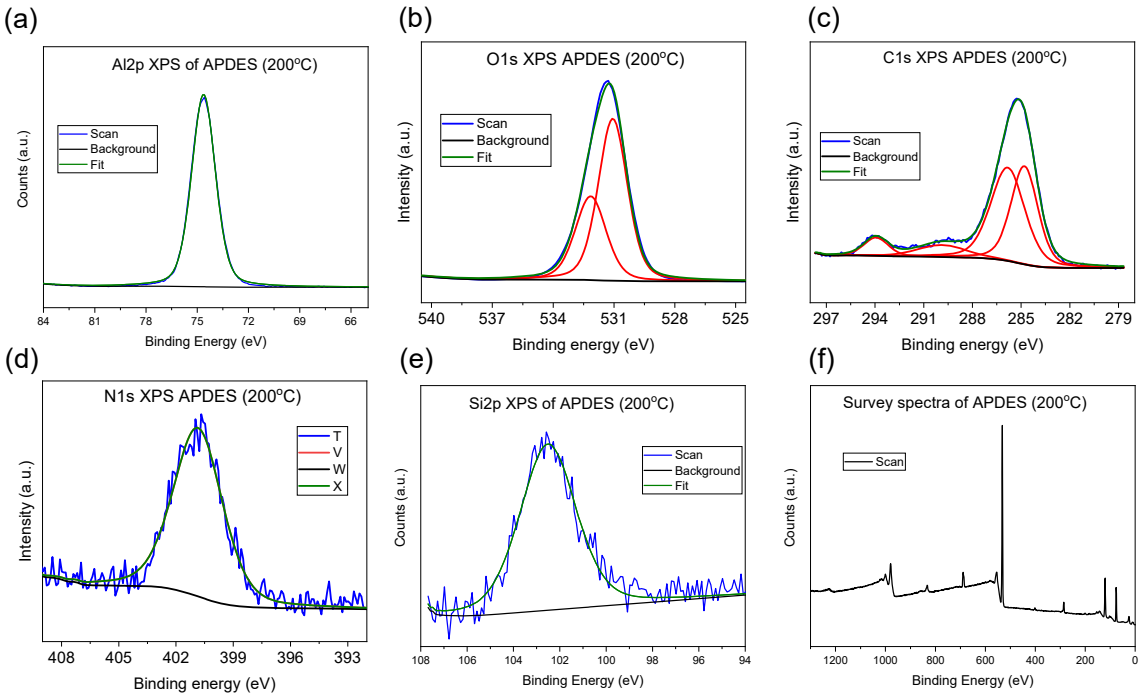

Figure S8. XPS spectra of 3-aminopropyldiethoxymethylsilane (APDES) grafted to ALD Al_2O_3 at 200°C. (a) Al2p, (b) O1s, (c) C1s, (d) N1s, (e) Si2p, (f) Survey spectrum.

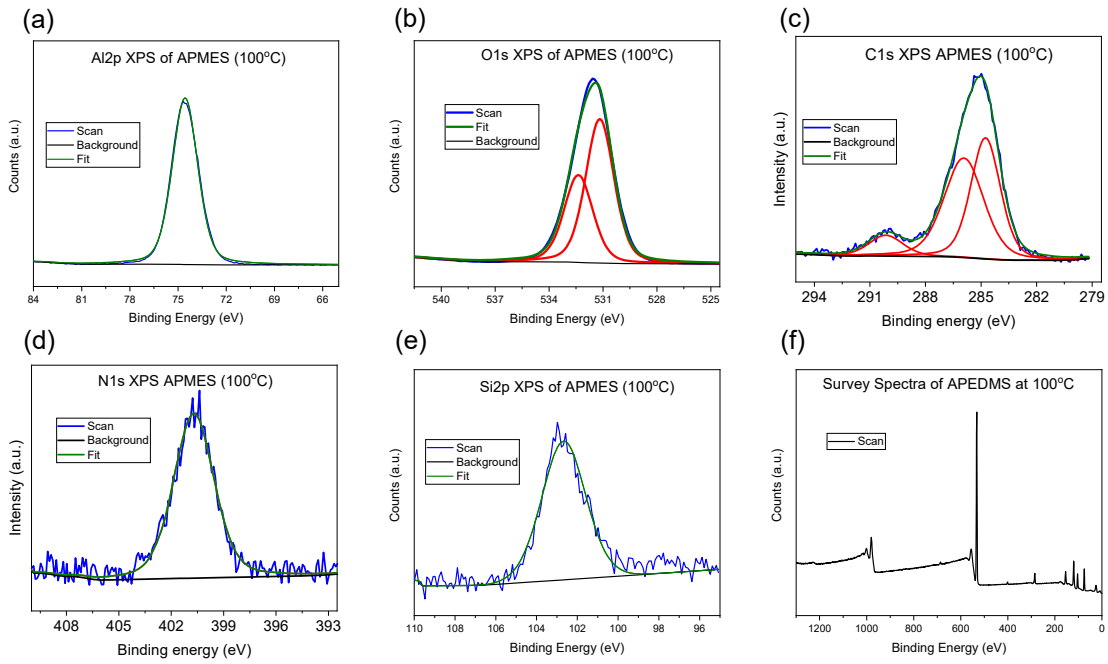

Figure S9. XPS spectra of 3-aminopropylmonoethoxydimethylsilane (APMES) grafted to ALD Al_2O_3 at 100°C. (a) Al2p, (b) O1s, (c) C1s, (d) N1s, (e) Si2p, (f) Survey spectrum.

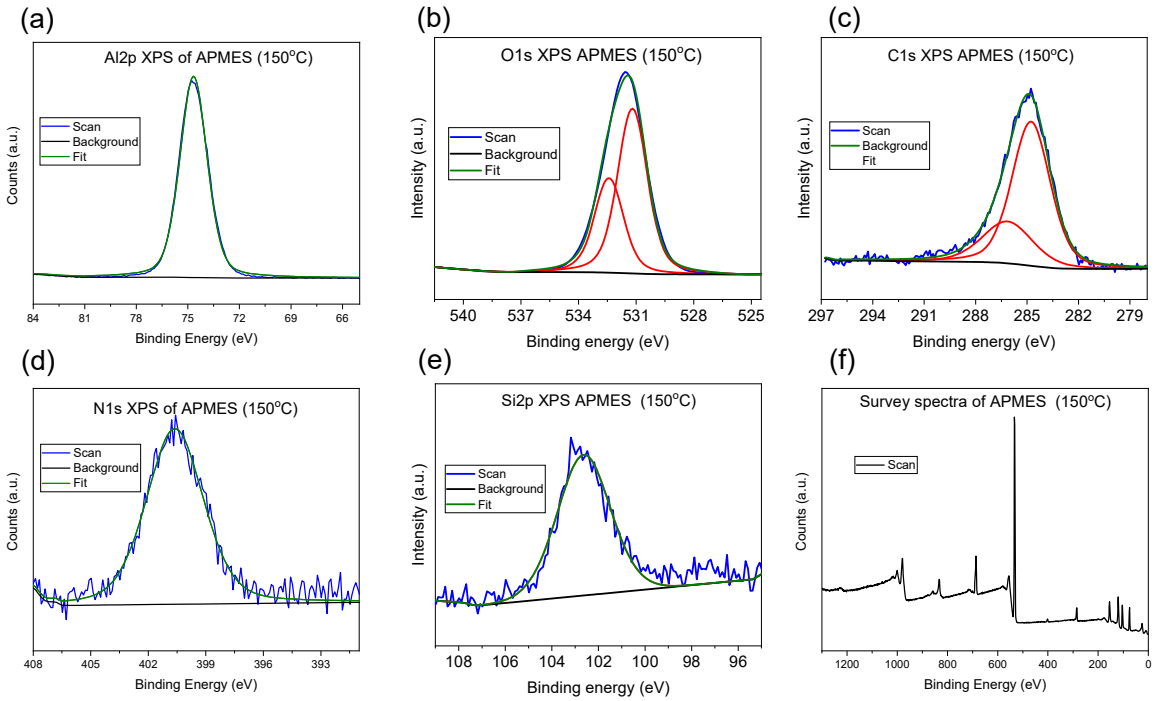

Figure S10. XPS spectra of 3-aminopropylmonoethoxydimethylsilane (APMES) grafted to ALD Al_2O_3 at 150°C. (a) Al2p, (b) O1s, (c) C1s, (d) N1s, (e) Si2p, (f) Survey spectrum.

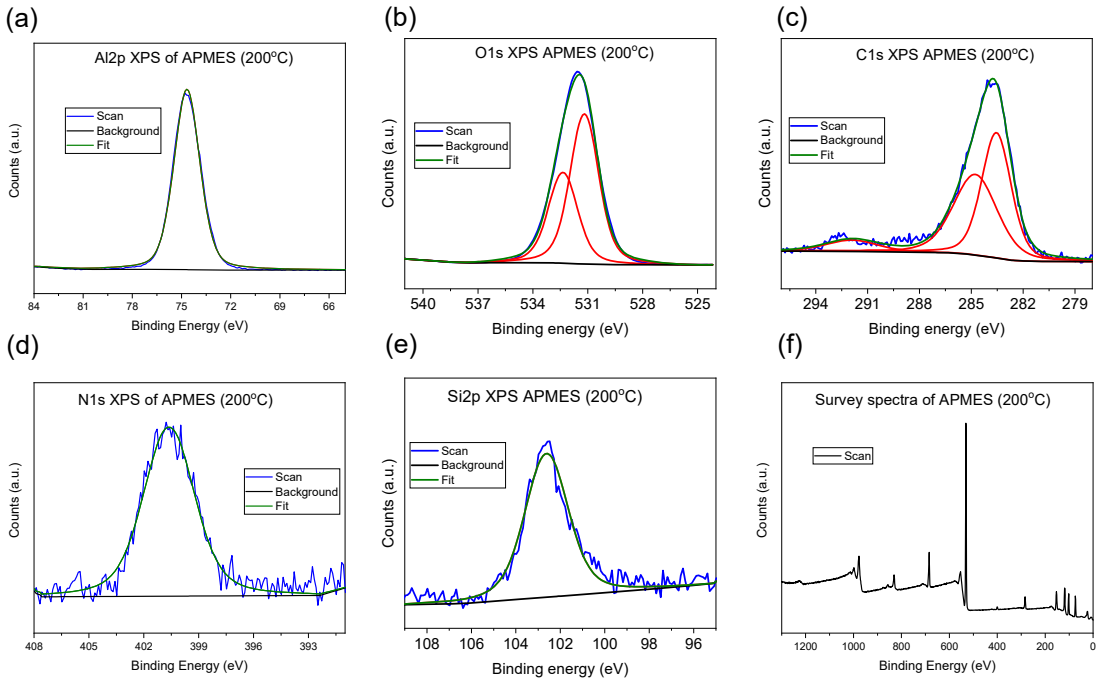

Figure S11. XPS spectra of 3-aminopropylmonoethoxydimethylsilane (APMES) grafted to ALD Al_2O_3 at 200°C. (a) Al2p, (b) O1s, (c) C1s, (d) N1s, (e) Si2p, (f) Survey spectrum.

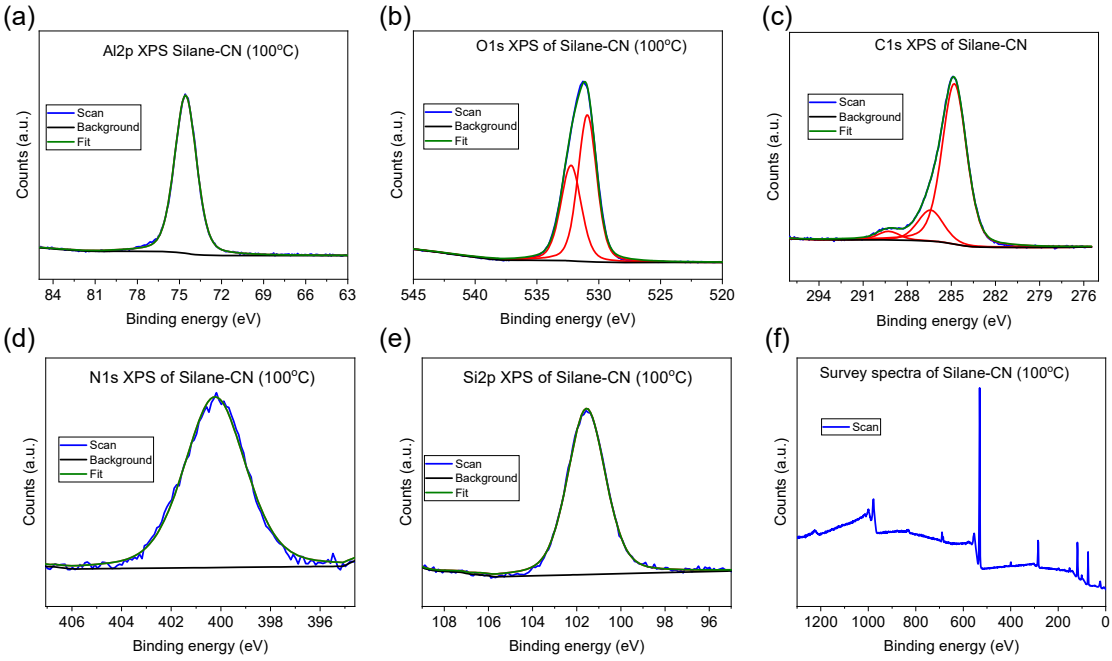

Figure S12. XPS spectra of 3-cyanopropyltrichlorosilane (Silane-CN) grafted to ALD Al_2O_3 at 100°C. (a) Al2p, (b) O1s, (c) C1s, (d) N1s, (e) Si2p, (f) Survey spectrum.

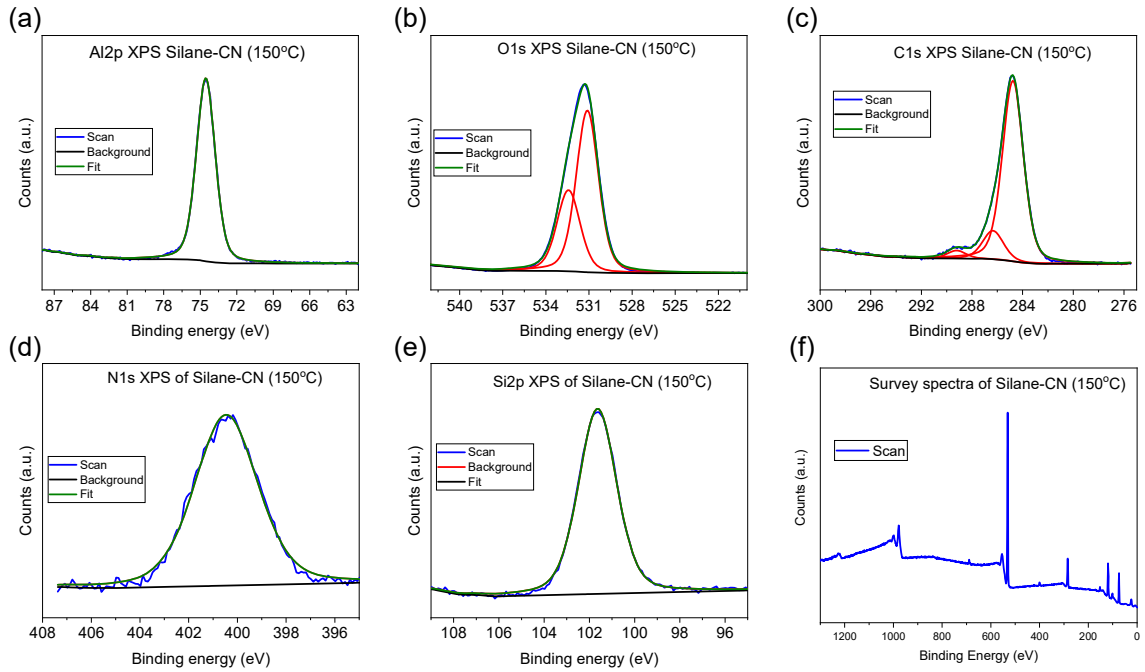

Figure S13. XPS spectra of 3-cyanopropyltrichlorosilane (Silane-CN) grafted to ALD Al_2O_3 at 150°C. (a) Al2p, (b) O1s, (c) C1s, (d) N1s, (e) Si2p, (f) Survey spectrum.

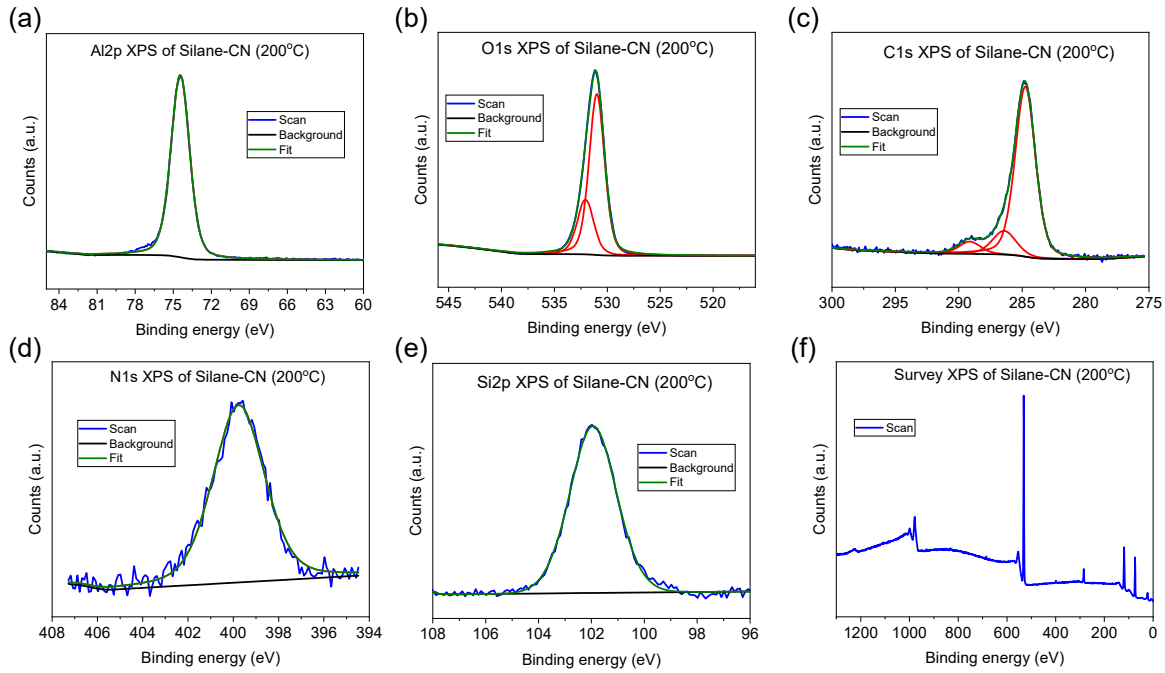

Figure S14. XPS spectra of 3-cyanopropyltrichlorosilane (Silane-CN) grafted to ALD Al_2O_3 at 200°C. (a) Al2p, (b) O1s, (c) C1s, (d) N1s, (e) Si2p, (f) Survey spectrum.

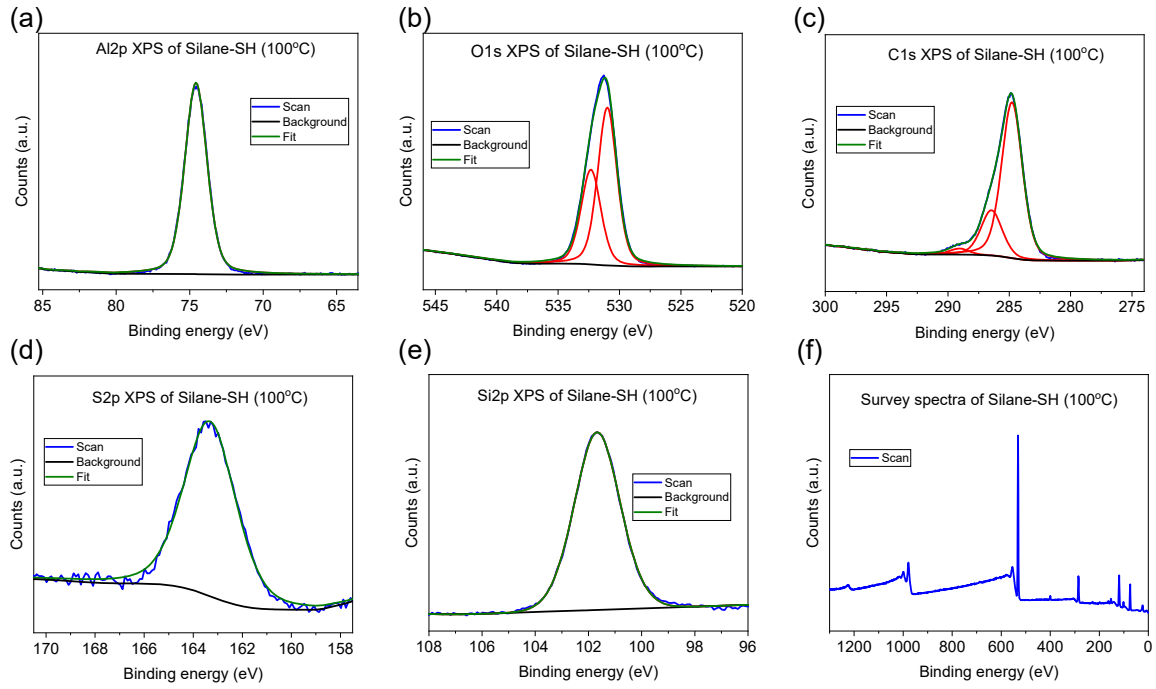

Figure S15. XPS spectra of 3-mercaptopropyltriethoxysilane (Silane-SH) grafted to ALD Al_2O_3 at 100°C. (a) Al2p, (b) O1s, (c) C1s, (d) S2p, (e) Si2p, (f) Survey spectrum.

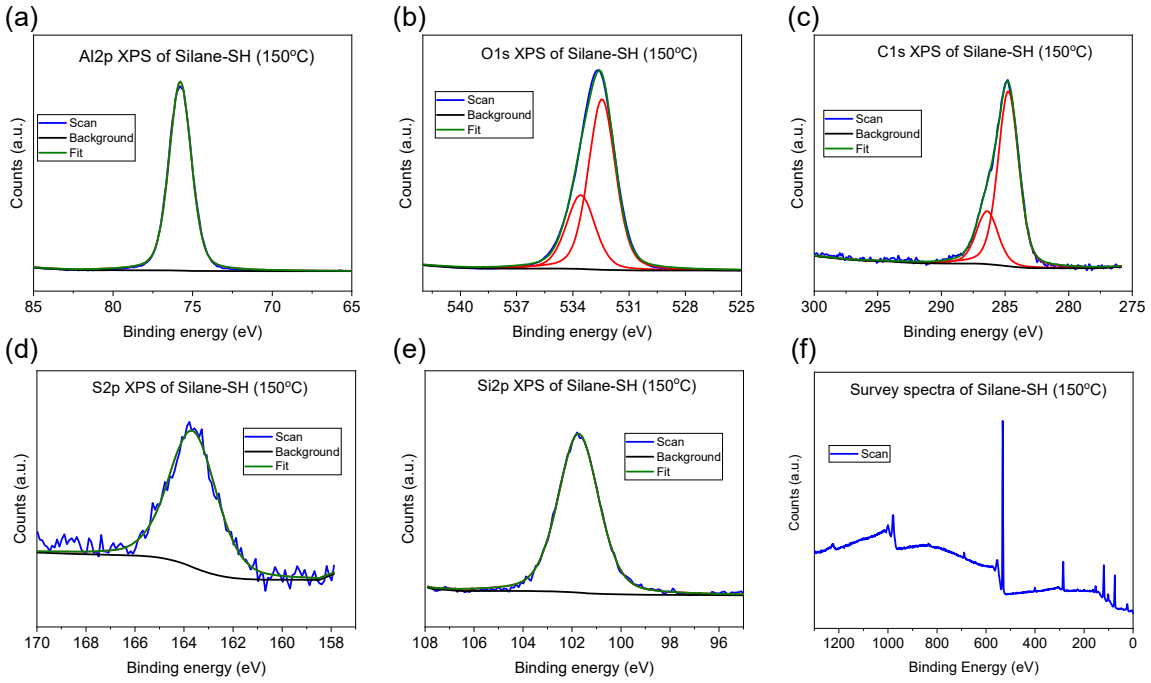

Figure S16. XPS spectra of 3-mercaptopropyltriethoxysilane (Silane-SH) grafted to ALD Al_2O_3 at 150°C. (a) Al2p, (b) O1s, (c) C1s, (d) S2p, (e) Si2p, (f) Survey spectrum.

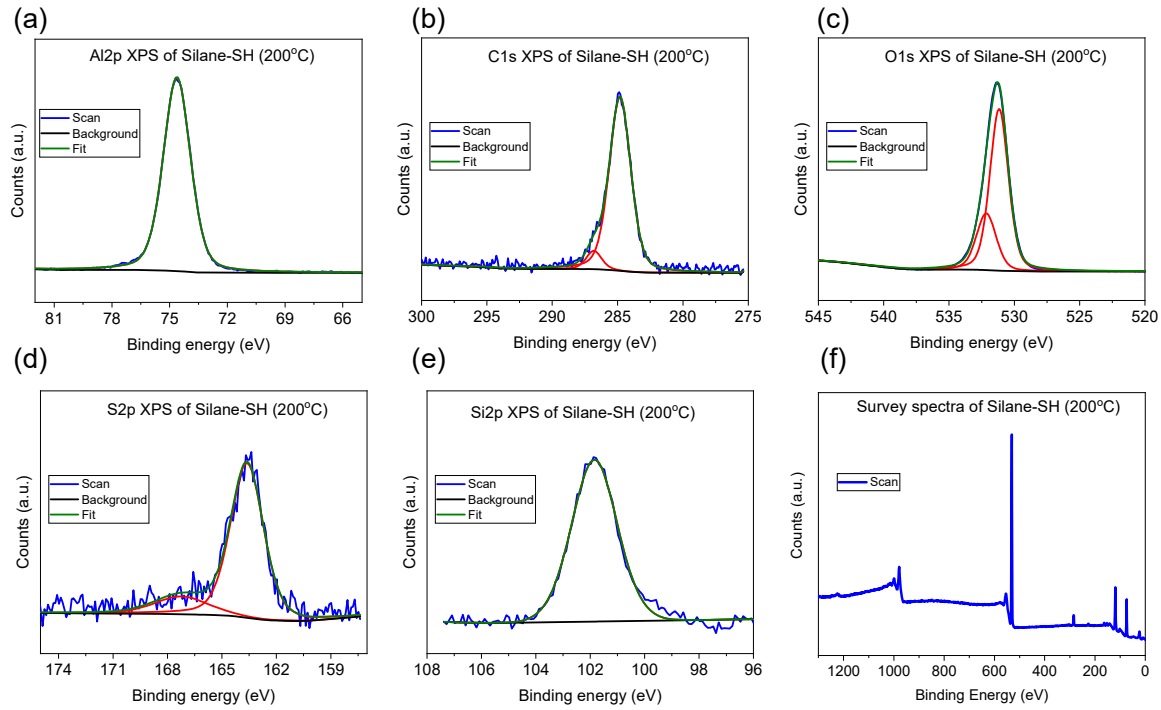

Figure S17. XPS spectra of 3-mercaptopropyltriethoxysilane (Silane-SH) grafted to ALD Al_2O_3 at 200°C. (a) Al2p, (b) O1s, (c) C1s, (d) S2p, (e) Si2p, (f) Survey spectrum.

VI. IN SITU FTIR MEASUREMENTS

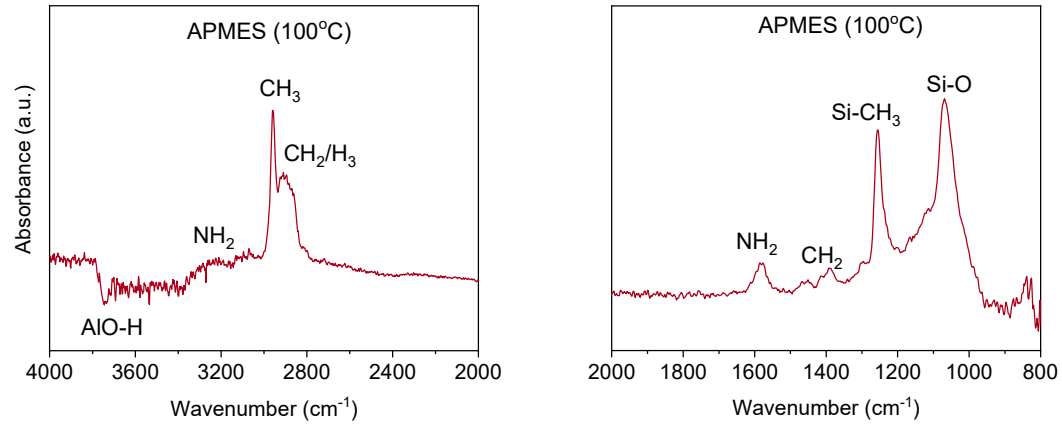

Figure S18. In situ FTIR spectra of 3-aminopropylmonoethoxydimethylsilane (APMES) grafted to ALD Al_2O_3 at 100°C.

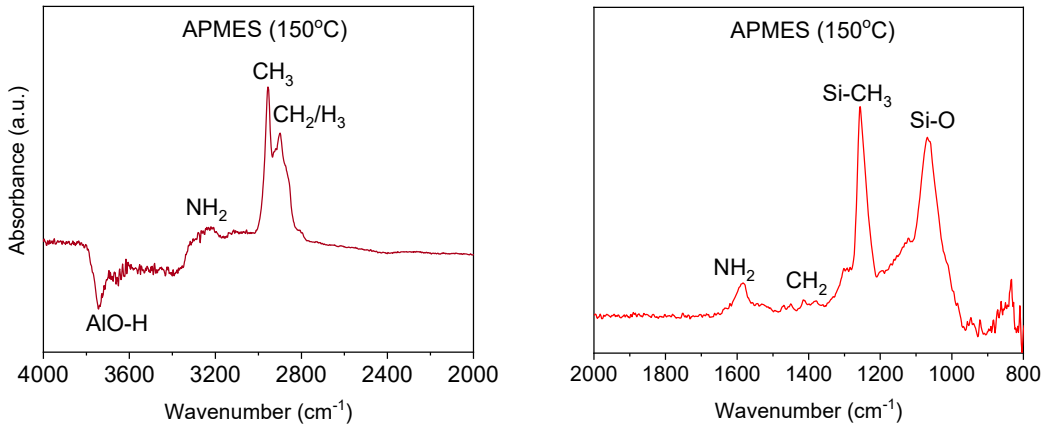

Figure S19. In situ FTIR spectra of 3-aminopropylmonoethoxydimethylsilane (APMES) grafted to ALD Al_2O_3 at 150°C.

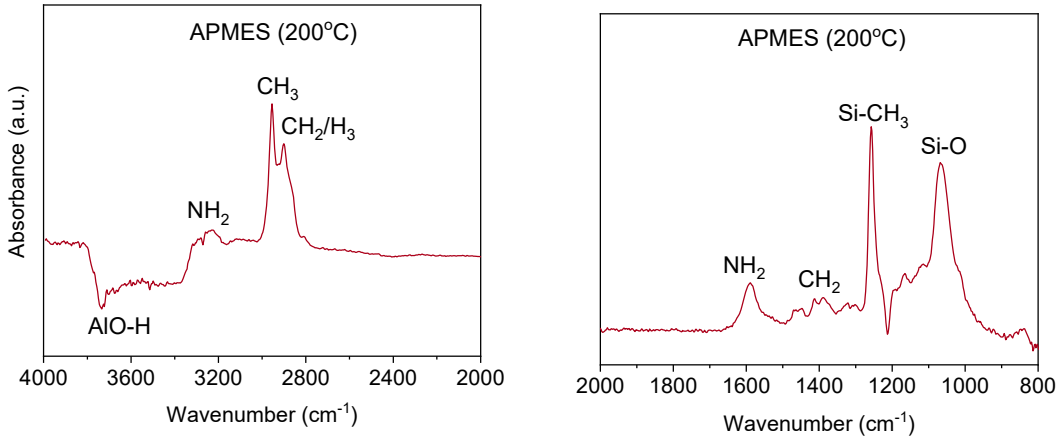

Figure S20. In situ FTIR spectra of 3-aminopropylmonoethoxydimethylsilane (APMES) grafted to ALD Al_2O_3 at 200°C.

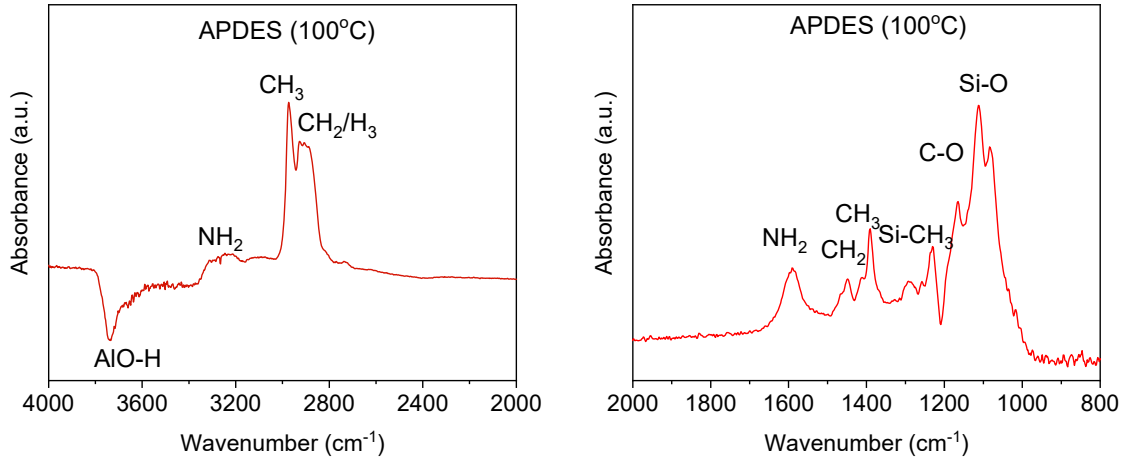

Figure S21. In situ FTIR spectra of 3-aminopropyldiethoxymethylsilane (APDES) grafted to ALD Al_2O_3 at 100°C.

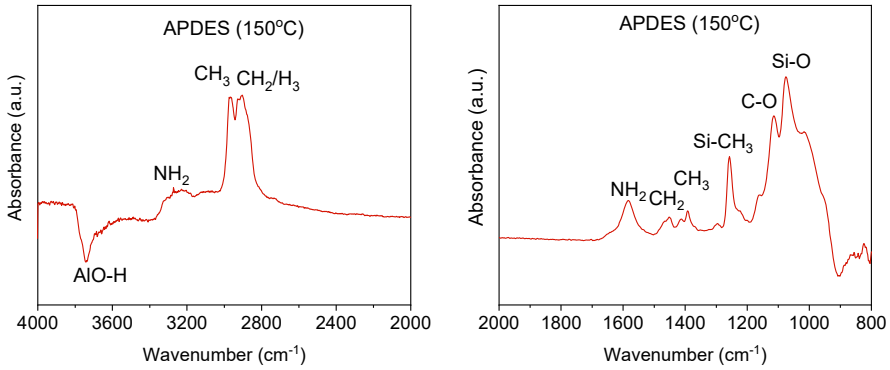

Figure S22. In situ FTIR spectra of 3-aminopropyldiethoxymethylsilane (APDES) grafted to ALD Al_2O_3 at 150°C.

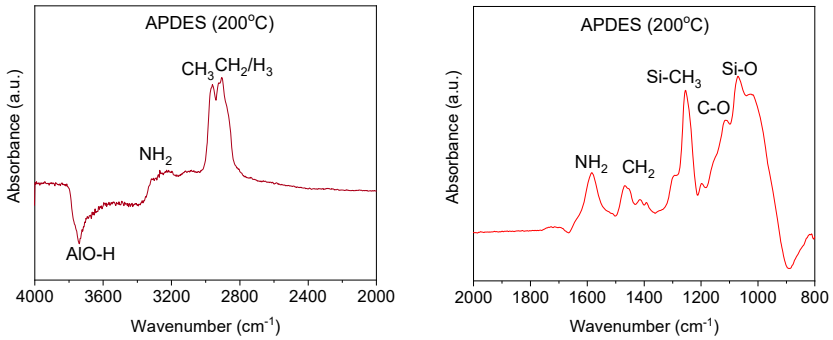

Figure S23. In situ FTIR spectra of 3-aminopropyldiethoxymethylsilane (APDES) grafted to ALD Al_2O_3 at 200°C.

VII. SURFACE INHIBITION OF APTES REACTION BY RELEASED ETHANOL

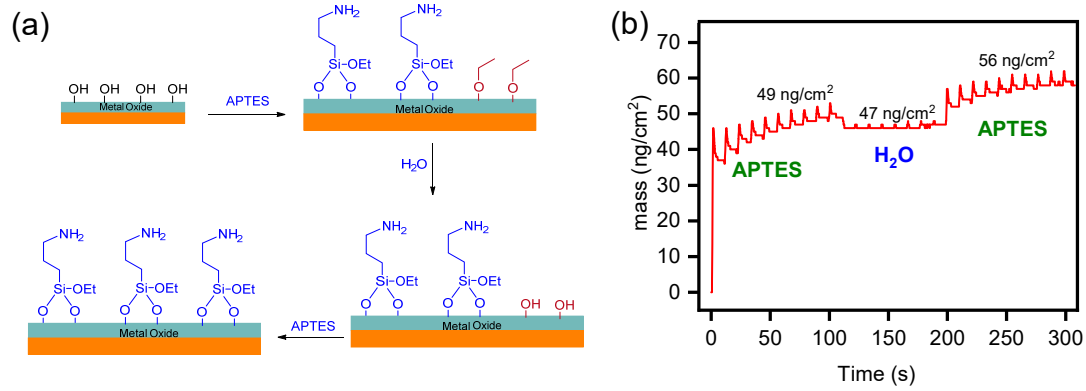

Figure S24. (a) Schematic illustration of surface inhibition of APTES reaction on ALD Al_2O_3 by released ethanol followed by APTES reaction. (b) In situ quartz crystal microbalance (QCM) measurement for 10 cycles of APTES (1s:10s), 10 cycles of water (1s:10s) and 10 cycles (1s:10s) of APTES.

VIII. Elemental Composition of films

Table SI. Elemental composition of films from XPS measurements.

Samples	T (°C)	Al2p	O1s	C1s	Si2p	N1s	S2p	Cl2p
200xAl_2O_3	150	34.37	56.76	8.87	-	-	-	-
APDES	100	32.93	54.45	8.63	2.03	1.96	-	-
	150	33.14	53.79	8.95	2.01	2.02	-	-
	200	32.91	53.63	9.35	2.07	2.04	-	-
APMES	100	32.86	52.79	9.21	2.58	2.56	-	-
	150	32.82	52.44	9.45	2.64	2.65	-	-
	200	32.53	52.26	9.71	2.71	2.79	-	-
CN-Silane	100	32.68	52.69	10.21	1.62	1.58	-	1.22
	150	32.37	52.63	10.13	1.92	1.86	-	1.09
	200	32.48	52.54	9.98	2.08	2.01	-	0.91
HS-Silane	100	33.69	53.80	9.76	1.70	-	1.05	-
	150	33.89	53.85	9.71	1.52	-	1.03	-
	200	33.82	53.92	9.79	1.45	-	1.02	-